REPUBLIC OF TÜRKİYE
ACIBADEM MEHMET ALİ AYDINLAR UNIVERSITY
INSTITUTE OF NATURAL AND APPLIED SCIENCES

LAMP BASED SCREENING KIT DEVELOPMENT TO DETECT SMA FROM SALIVA

ÖZDEYİŞ HÜLYA İŞGÖRDÜ

MASTER THESIS

DEPARTMENT OF MOLECULAR
BIOLOGY AND GENETICS

SUPERVISOR
Prof. Eda Tahir Turanlı

CO-ADVISOR
Prof. Osman Uğur Sezerman

İSTANBUL-2024

REPUBLIC OF TÜRKİYE
ACIBADEM MEHMET ALİ AYDINLAR UNIVERSITY
INSTITUTE OF NATURAL AND APPLIED SCIENCES

LAMP BASED SCREENING KIT DEVELOPMENT TO DETECT SMA FROM SALIVA

ÖZDEYİŞ HÜLYA İŞGÖRDÜ

MASTER THESIS

DEPARTMENT OF MOLECULAR
BIOLOGY AND GENETICS

SUPERVISOR
Prof. Eda Tahir Turanlı

CO-ADVISOR
Prof. Osman Uğur Sezerman

İSTANBUL-2024

DECLARATION

I declare that this thesis work is my own work, I had no unethical behavior at any stages from the planning to the writing of the thesis, I obtained all the information in this thesis in accordance with academic and ethical rules, I cited all the information and comments that were not obtained with this thesis work, and I provided resources in the list of references. I also declare that there was no violation of any patents and copyrights during the study and writing of this thesis.

22.08.2024
Özdeyiş Hülya İşgördü

PREFACE AND ACKNOWLEDGMENTS

First and foremost, I would like to express my heartfelt gratitude to my advisor, Prof. Eda Tahir Turanlı, for her unwavering guidance, endless patience, and constant support throughout my early research career and the entirety of this project. Prof. Eda Tahir Turanlı has not only been an exceptional advisor but also a highly successful scientist, a wonderful mentor, and a kind and compassionate person. She has always been a supportive and encouraging role model in my scientific life.

I also wish to extend my deepest thanks to my co-advisor, Prof. Osman Uğur Sezerman, for his valuable support at every stage of my thesis, for encouraging me, and for always being by my side during the most important moments of my life. Throughout my life, I will remain deeply grateful to my teacher Uğur, who has been a cornerstone of both my undergraduate and graduate education. His guidance has left an indelible mark on my academic journey and personal growth. Being one of his students has been a great privilege and honor for me.

I am grateful to Assoc. Prof. Dr. Pınar Topaloğlu from Istanbul University-Çapa Hospital for her contributions and support in facilitating this research by providing samples and also i would like to thank being my committee member and her scientific critiques and constructive feedback. I am grateful to individuals with SMA and their precious families for agreeing to provide the samples tested in the thesis and for their contribution to science.

I would like to thank my committee member Prof. Emel Timuçin from Acıbadem Mehmet Ali Aydınlar University for her scientific critiques and constructive feedback. I am especially grateful to her for helping me with all my questions regarding statistical calculations and giving me motivation throughout the thesis process. Additionally, I am grateful to my alternate committee members, Assoc. Prof. Dr. Ahmet Can Timuçin from Acıbadem Mehmet Ali Aydınla University and Prof. Pınar Ata from Marmara University, for their support, scientific critiques and constructive feedback.

This thesis was financially supported by the TÜSEB Strategic Research and Development Support Program as part of the 2021-SMA-ARGE call, project number 11662, in collaboration with the Acıbadem Mehmet Ali Aydınlar University Project Office. I would like to extend my thanks to the Turkish Institutes of Health for funding this research. I also wish to express my appreciation to the project office officials for all their support.

I am deeply thankful to my colleague, Abdullah Alper Bülbül, for his contributions and all his support throughout this project. My gratitude also goes to my teammates in the Sezerman Laboratory, Milena Jakimovska Özdemir, İbrahim Sertdemir and Dr. Tayyip Karaman, for their exceptional efforts in forming the project idea and their unlimited support whenever I needed help. I am grateful to Ali Arslan for his assistance with the wet-lab work and his patience in answering all my questions. I also wish to thank Özlem Sil for her support during the wet-lab process. I would like to thank Zeynep Şevval Düvenci, Dilanur Kamali and Sinan Abus for the morale and support they provided throughout my thesis process.

Special thanks to my friend from undergraduate studies, Zeynep Beyza Akpek, for being a wonderful aunt to my son and a fantastic sister to me, and of course, for being one of the facilitators of this process.

I am deeply grateful to my precious family, who unwaveringly supported me throughout my entire educational journey, including my master's degree. I especially want to thank my son Aslan, who was born during my thesis period, my husband and my mother. Their presence by my side made this success possible, and I could not have achieved it without them.

To my son

TABLE OF CONTENTS

LIST OF ABBREVIATIONS AND SYMBOLS

°C	Centigrade Degree
ATADEK	Acıbadem Mehmet Ali Aydınlar University Medical Research Evaluation Board
ATP	Adenosine Triphosphate
B3	Backward Primer
BIP	Backward Internal Primer
bp	Base Pair
CI	Confidence Interval
CK	Creatine Kinase
CNS	Central Nervous System
-d(RFU)/dT	Time-Dependent Derivative of Relative Fluorescence Units
DNA	Deoxyribonucleic Acid
dNTPs	Deoxyribonucleotide Triphosphate
EMG	Electromyography
ER	Endoplasmic Reticulum
F3	Forward Primer
FIP	Forward Internal Primer
kb	Kilobase
kcal/mol	Kilocalorie Per Mole
LAMP	Loop-Mediated Isothermal Amplification
LB	Loop Primer Backward
LF	Loop Primer Forward
MgSO4	Magnesium Sulfate
MLPA	Multiplex Ligation Dependent Probe Amplification
mRNA	Messenger RNA
mRNP	Messenger Ribonucleoprotein
NGS	Next Generation Sequencing
NMJ	Neuromuscular Junction
NPV	Negative Predictive Value
OMIM	Online Mendelian Inheritance in Man
PCR	Polymerase Chain Reaction

PPV	Positive Predictive Value
RFU	Relative Fluorescence Units
RNA	Ribonucleic Acid
RT qPCR	Quantitative Real-Time PCR
RT-PCR	Real Time Polymerase Chain Reacion
SARS-CoV-2	Severe Acute Respiratory Syndrome Coronavirus 2
SMA	Spinal Muscular Atrophy
SMN	Survival Motor Neuron Protein
SMN1	Survival Motor Neuron 1
SMN2	Survival Motor Neuron 2
SNPs	Single Nucleotide Polymorphism
snRNPs	Small Nuclear Ribonucleoproteins
Tm	Melting Temperature
TMEM41B	Transmembrane Protein 41B
U / ml	Units Per Milliliter
UTR	Untranslated Region
UV	Ultraviolet
δ	Delta
ΔG	Gibbs free energy change

LIST OF FIGURES

LIST OF TABLES

SUMMARY

LAMP Based Screening Kit Development to Detect SMA From Saliva

This study aimed to develop a saliva screening kit based on Loop-mediated isothermal amplification (LAMP) for early diagnosis and carrier screening of Spinal Muscular Atrophy (SMA). SMA is a rare genetic disease commonly associated with mutations in the SMN1 (Survival Motor Neuron 1) gene, typically manifesting during infancy and resulting in the death of motor neurons. In this regard, customized primer sets were designed to target the specific SMN1:c.840C>T rs1164325688 variation in the SMN1 gene and the homozygous deletion in the 7th exon region of the SMN1 gene to detect SMA patients and carriers. The primer sets in the developed kit are designed to strongly amplify the 7^{th} exon region of the SMN1 gene in healthy individuals. In carriers, due to a single-copy mutation or deletion in the SMN1 gene, this amplification signal will be approximately 50% less compared to healthy individuals. In patients, who have a double-copy mutation or deletion in the SMN1 gene, the amplification will either be absent or significantly reduced. These primer sets have been optimized and rigorously tested to ensure precise and reliable amplification across different genotypic profiles. The newly developed screening kit for SMA demonstrated 82.35% sensitivity and 83.33% specificity when evaluated using saliva samples from 18 patients, 16 carriers, and 18 healthy individuals. These results indicate that the kit is highly accurate in identifying both SMA patients and carriers, making it a valuable tool for early diagnosis and intervention of the disease.

Keywords: Early diagnosis, LAMP, Saliva screening kit, SMN1 Gene, Spinal Muscular Atrophy.

ÖZET

LAMP Tabanlı Tükürükten SMA Tarama Kiti Geliştirilmesi

Bu çalışma, Spinal Musküler Atrofi (SMA) hastalığının erken teşhisi ve taşıyıcı taraması için ilmiğe dayalı izotermal çoğaltma yöntemi (LAMP) tabanlı bir tükürük tarama kiti geliştirme amacıyla yapılmıştır. SMA, genellikle SMN1 (Survival Motor Neuron 1) genindeki mutasyonlarla ilişkilendirilen nadir görülen genetik bir hastalıktır, özellikle bebeklik döneminde görülmektedir ve motor nöronların ölümü ile sonuçlanmaktadır. Bu doğrultuda, SMN1 genindeki spesifik SMN1:c.840C>T rs1164325688 varyasyonu ve SMN1 geninin 7. ekzom bölgesindeki homozigot delesyonu hedef alınarak SMA hastalarını ve taşıyıcılarını tespit etmek için özelleştirilmiş primer setleri tasarlanmıştır. Geliştirilen kitin primer setleri, sağlıklı bireylerin SMN1 geninin 7. ekzom bölgesini güçlü bir şekilde çoğaltacak şekilde tasarlanmıştır. Taşıyıcılarda ise SMN1 geninde tek kopya mutasyon veya delesyon olduğu için bu çoğaltma sinyali sağlıklı bireylere kıyasla yaklaşık %50 daha az olacaktır. Hastalarda, SMN1 geninde çift kopya mutasyon veya delesyon bulunduğundan, çoğaltma ya hiç gerçekleşmeyecek ya da çok az olacaktır. Bu primer setleri, farklı genotip profilleri arasında kesin ve güvenilir çoğaltma sağlamak için optimize edilmiş ve titizlikle test edilmiştir. SMA için yeni geliştirilen tarama kiti, 18 hasta, 16 taşıyıcı ve 18 sağlıklı kişiden alınan tükürük örnekleri kullanılarak değerlendirildiğinde %82,35 duyarlılık ve %83,33 özgüllük gösterdi. Bu sonuçlar, kitin hem SMA hastalarını hem de taşıyıcıları belirlemede son derece doğru olduğunu ve hastalığın erken teşhisi ve müdahalesi için onu değerli bir araç haline getirdiğini gösteriyor.

Anahtar Sözcükler: Erken teşhis, LAMP, SMN1 geni, Spinal Musküler Atrofi, Tükürük tarama kiti.

1. INTRODUCTION

Spinal muscular atrophy stands as a profound genetic affliction, characterized by its impact on motor neurons, often leading to severe physical debilitation. Typically emerging in infancy, SMA progressively deteriorates muscle function, potentially culminating in life-threatening conditions. (1) Timely diagnosis and intervention are pivotal in mitigating its advancement and enhancing patient well-being. However, conventional diagnostic modalities are frequently protracted, intrusive, and financially burdensome. Against this backdrop, this study endeavors to pioneer a novel approach through the development of a saliva screening kit based on LAMP. Renowned for its swift outcomes and exceptional accuracy, the LAMP method offers promise for expediting diagnostics while circumventing invasive procedures. (2) The principal aim of this investigation is to conceptualize, refine, and validate an innovative screening toolkit adept at swiftly and accurately identifying both SMA patients and carriers. Such a breakthrough promises to streamline genetic screening protocols, fostering early detection and informed decision-making. By navigating the complexities of SMA diagnosis with precision and efficiency, this research aspires to foster a paradigm shift in the clinical landscape, underlining the potential for transformative advancements in genetic screening practices and patient care.

1.1. Spinal Muscular Atrophy

Neurodegeneration is usually identified by the decline of groups of nerve cells and the disruption of their connections, within the central nervous system. This process ultimately results in the loss of functions. (3)

Spinal muscular atrophy is a hereditary condition that follows an autosomal recessive pattern. It is mostly caused by mutations in the SMN1 gene located on chromosome 5. These abnormalities result in decreased production of the survival

motor neuron protein (SMN). This leads to the malfunction and deterioration of α-motor neurons in the spinal cord and brainstem, as well as the gradual wasting and weakening of muscles in the limbs, trunk, bulbar region (which governs swallowing), and respiratory muscles. Additionally, it results in progressive muscle wasting and dysfunction and degeneration of alpha motor neurons in the cord and brainstem. (4)

Traditionally SMA has been categorized into two forms: one with prenatal onset (type 0) and another with adult onset featuring a milder presentation (type 4). The three main types of SMA begin during childhood (types 1 to 3). (4)

The prevalent Type I form known as Werdnig disease is more severe compared to other types typically starting before a babys sixth month and leading to death within the first two years. Type II generally begins, between 6 to 18 months resulting in affected children being unable to walk or stand. Type III, also known as Wohlfart Kugelberg Welander disease typically manifests in children within their years or even, during adolescence. These individuals can. May encounter difficulties when trying to stand up. Type IV represents the form of the condition. Often goes unnoticed until adulthood. (5)

Furthermore, a recent discovery, Type 0 is a variation that usually leads to death within the first few weeks after birth. This classification system is primarily based on the age at which symptoms appear and the highest level of motor function achieved without intervention. (6)

An excellent example of this can be seen in SMA type 1 (OMIM 253300), which is

the most common subtype of SMA. Without treatment, individuals with this subtype experience symptoms before 6 months of age, are unable to sit independently, and rapidly deteriorate in terms of motor skills, respiratory function, and bulbar function. The mortality rate for this subtype is over 90% by the age of 2.

In contrast, most newborns diagnosed with SMA type 1 who get treatment have a survival rate of over two years. Moreover, if treatment is administered promptly after diagnosis, these infants often see improvements in their functionality and reach developmental milestones that are not seen in untreated infants (7).

1.1.1. Epidemiology

Approximately one, out of every ten thousand births or between 7,8 to 10 out of every 100.000 live births are diagnosed with SMA. (8-11) The occurrence of SMA ranges from 4 - 10 cases per 100000 births. Ranks as the second most prevalent after Duchenne Muscular Dystrophy among pediatric neuromuscular diseases. The frequency of carriers bearing SMN1 gene mutations for SMA ranges from 1 in every 47 to 1 in every 90 individuals. SMA stands as the cause of infant mortality and is notably the second most common genetic cause of infant death following cystic fibrosis in terms of fatality. (12-14)

As detailed in the SMA Clinical Protocol issued by the Ministry of Health in Türkiye during June 2022 an average of 150 infants are born with SMA annually in Türkiye. The protocol underscores that implementing screening will facilitate early-stage treatment for this disease. In Türkiye in the year 2022 there were three thousand individuals affected by SMA. Considering an average of around 1200000 births in Türkiye it is estimated that between 130 babies (with an average figure of around 150) are born with SMA each year. (15)

1.1.2. Genetics

In 1990, the mapping of all three kinds of SMA was accomplished, locating them precisely on chromosome 5q11.1–13.3. This intricate area has a substantial 500-kb duplication and includes the telomeric SMN1 gene, which encodes SMN, as well as its centromeric paralogue, SMN2. (16-17)

The SMN gene consists of nine exons, which are exons 1, 2a, 2b, 3, 4, 5, 6, 7, and 8. Exon 8 encodes the 3' untranslated region (UTR). Typically, SMN1 pre-mRNAs undergo splicing to maintain all exons. A solitary operative, coding mutation c.840C>T in exon 7 of SMN2 renders an exonic splicing enhancer non-functional and concurrently generates an exonic splicing silencer. This alteration is functionally inconsequential in terms of the protein's structure, but it has an impact on the process of splicing, causing the exclusion of exon 7 from the majority of SMN2 transcripts. As a consequence, the resultant SMN protein is truncated and undergoes fast degradation. Due to occasional retention of exon 7, each instance of SMN2 generates about 10% of fully intact and operational SMN. The symptoms of SMA, including as the delayed growth and degeneration of α-motor neurons, are caused by decreased levels of the SMN protein. (18-20)

Approximately 95% of individuals diagnosed with 5q-SMA have homozygous deletions of either exons 7 and 8, or only exon 7, in the SMN1 gene, irrespective of the disease's manifestation. Some patients have a specific genetic mutation in one of their SMN1 alleles, together with a deletion in the other SMN1 allele. In extremely rare cases, patients may have mutations in either of the SMN1 exons in both alleles. De novo mutations have a very high occurrence rate of around 2% due to the instability of the 5q region. Patients with milder forms of spinal muscular atrophy (SMA kinds 2 and 3) often experience gene conversion, when the SMN1 exon 7 is changed to that of SMN2,

instead of actual deletions of SMN1, as are seen in SMA type 1. Conversely, the occurrence of SMN2 gene conversion into SMN1 may also take place (21-22).

1.1.3. SMN2 Expression and Splicing

Both SMN1 and SMN2 are consistently active in transcription and are controlled by multi-kilobase promoters, transcription factors, epigenetic factors, and long non-coding RNAs.

The transcriptional activity of both genes may be influenced by the developmental stage, cell stress, and autoregulatory mechanisms. It is important to mention that in the early stages of developing treatments for SMA, the main emphasis was on using small molecules to activate the transcription of SMN2. However, the drugs that were tested were not strong enough, specific enough, or safe enough to be utilized for long-term treatment. The level of transcriptional activity of SMN2 controls the amount of pre-mRNA accessible for splice-modulating treatments. Since splicing usually happens at the same time as transcription, the combination of transcriptional and splice-modifying therapy is still a desirable objective. (23-33)

The process of alternative splicing of SMN2 exon 7 plays a vital role in the development of spinal muscular atrophy. Exon 7 splicing is regulated by several factors, including cis-acting motifs located within introns and exons that increase or silence splicing, as well as trans-acting factors such as RNA-binding proteins. The severity of human diseases may be reduced by certain genetic variations called single-nucleotide polymorphisms, which affect the balance of these factors. An instance of a single base substitution, namely c.859G>C, occurs in the exon 7 encoding sequence of SMN2. This alteration leads to the creation of a novel exonic splicing enhancer element, which in turn leads to an increase in full-length transcripts and a decrease in the severity of the

condition. Changes in the quantity of certain RNA-binding proteins might potentially alter the severity of a disease. The frequency of exon 7 inclusion may vary depending on the kind of cell. Normal motor neurons in the spinal cord produce lower quantities of full-length SMN mRNA from SMN2 compared to other cells. The improper inclusion of SMN2 exon 7 in motor neurons may lead to significantly reduced amounts of SMN in these cells, making them more susceptible to illness. (34-42)

The relationship, between the number of SMN2 copies and the severity of SMA is intricate and multifaceted. Individuals who do not have atrophy (SMA) typically have at least one working SMN1 gene but the number of SMN2 copies they have can differ. 10–15% of individuals do not have any SMN2 copies. In SMA patients there is a relationship, between the number of SMN2 copies and the severity of the disease. For instance, in a study involving participants researchers observed how SMN2 copies were distributed among different types of SMA. 80% of those with SMA type 1 had one or two copies of SMN2 while 78% of type 2 patients had three copies. In contrast most patients with type 3 had three or four copies, with around 93% showing this pattern. However, predicting the impact of SMA based on the number of SMN2 copies is not straightforward especially for types 2 and 3. There are instances where individuals with SMA types 1, 2 or 3 possess two or three copies of SMN2. Furthermore, cases exist where five SMN2 copies were found in family members who had two working SMN1 genes and in type 3 SMA patients. These findings indicate that although the number of SMN2 copies plays a role, in determining disease severity for SMA it is not the factor involved. Additional genes that influence the range of symptoms, in SMA, like PLS3 and NCALD have been recognized (43-52).

1.1.4. SMN Structure and Function

The SMN protein is essential, for cell functions in putting together small nuclear ribonucleoproteins (snRNPs) needed for pre mRNA splicing. It has binding regions and mutations affecting these areas can have serious effects. For example, mutations

like missense or small deletions seen in patients with compound heterozygosity highlight the significance of these regions in SMNs role. SMN mostly exists as an oligomer, formed by interacting with itself through the YG box and bonding with proteins like gemin 2 – gemin 8. This oligomerization is crucial for its stability and effectiveness. If SMN lacks exon 7 it becomes unstable due to reduced ability to form oligomers and develops a motif leading to degradation. Including exon 7 is vital for maintaining SMNs stability and functionality. SMN can create protein complexes with functions that likely contribute to diverse cellular processes such as RNA metabolism and transport. Posttranslational modifications of SMN can alter its location, strength and effectiveness playing a role, in regulating its activity based on signals. In cell types SMN is spread out in the cytoplasm. Also forms specific structures called gems within the nucleus. The number of stones is linked to the seriousness of illnesses, in fibroblasts taken from patients. Within neurons SMN is discovered in granules within axons, where it moves rapidly in both directions. This indicates that SMN plays roles in both the nuclear sections of cells as well as in neural activities. (53-65)

In this context SMN is a protein involved in aspects of RNA metabolism and cellular balance with its structure, grouping, placement and post translational changes being crucial for its proper operation. Disruption of SMN can result in conditions like SMA.

The main role of SMN involves preserving the accuracy of spliceosomal snRNP assembly for the U2 dependent and minor (U12 dependent) spliceosomes. A shortage of SMN causes a deficiency in the U12 complex leading to splicing issues in genes dependent on this complex. One such influenced gene is TMEM41B, which codes for stasimon, a protein situated at the reticulum (ER). Though stasimons function remains poorly understood changes, in its splicing pattern have been noticed in SMA mouse models marked by weakness and premature death. Interestingly using a method to

deliver full length stasimon has shown promise in preserving the connections, between motor neurons and their sensory receptors in mice with SMA hinting at a treatment approach. However, this technique does not prevent the loss of motor neurons itself indicating that SMAs underlying causes are complex and likely involve factors beyond stasimon. Furthermore, SMNs functions go beyond regulating splicing. It plays a role in forming complexes with mRNA binding proteins like mRNP transport granules, which help transport mRNA along axons and enable protein production at the tips of developing neurons for their growth and function. The potential decrease in mRNP granules in SMA patients is an area for investigation. Moreover, SMN is directly linked to processes such as gene transcription and protein synthesis. When these functions are disrupted due to SMN dysfunction it can contribute to the development of SMA and other conditions. Understanding the roles of SMN in cell function as well as dysfunction is vital for devising effective treatments for SMA and related disorders. (66-77)

The discovery of human disease modifier genes, such as PLS3 (which encodes plastin 3, an actin-binding protein) and NCALD (which encodes neurocalcin-δ, a calcium-binding protein), emphasizes the significance of actin cytoskeletal dynamics, synaptic vesicle release, and endocytosis as outcomes of SMN deficiency (78-97).

1.1.5. Impaired Motor Unit Development and Degeneration

The primary cause of skeletal muscular weakness in SMA is the impairment of the SMA motor unit, which consists of motor neurons and the muscle fibers they control. Analysis of human postmortem tissues and mice models reveals that early stages of the illness are marked by developmental deficiencies that impact the motor neuron cell body, axon, and target myofibers. Particular abnormalities include of delayed development of excitatory synaptic inputs in motor neurons and their firing patterns in adult motor neurons; expansion of motor axons radially, ensheathment and myelination by Schwann cells; enhancement of structural complexity in NMJ synapses

and higher quantal content; and growth of myofibers (98-105).

1.1.6. Clinical Manifestations

Individuals with SMA are diagnosed either when they exhibit symptoms or before they show any symptoms. Presymptomatic individuals are detected by genetic testing prompted by a positive family history of SMA or through population-based newborn screening.

While SMA has a range of phenotypic expression, the first symptoms vary greatly across different subtypes. Shared characteristics of SMA over the whole range of the condition include a specific kind of nerve damage affecting only motor neurons and their axons, resulting in a lack of reflexes and involuntary muscle twitches. Sensation remains intact, and there is a consistent pattern of muscle weakening that is most pronounced in the muscles closest to the body's core and in the muscles of the lower limbs. Infants diagnosed with SMA type 1 have severe symptoms, including significant muscle weakness and ongoing challenges with breathing and eating. In a limited subset of individuals (type 0), symptoms begin before birth with decreased or nonexistent fetal movements and severe manifestations after birth, such as contractures. those diagnosed with SMA type 2 have a muscle weakening pattern that is comparable to those with type 1, but less severe. Additionally, they consistently develop scoliosis and experience some level of respiratory impairment. The clinical manifestations in individuals with SMA type 3 tend to be less severe and mostly include a propensity to fall, weakness in the lower limbs, and weariness. However, around 50% of patients will have a loss of independent ambulation, often occurring during puberty. people with SMA type 3 or 4 generally have good cognitive function. However, recent research suggests that some people with SMA type 1 or 2 may have cognitive impairment. (106-110).

1.1.7. Diagnosis

In the past electromyography (EMG) and muscle biopsy were commonly used to diagnose SMA. EMG examines muscle activity to identify denervation and reinnervation patterns indicating motor neuron issues. Muscle biopsy involves analyzing muscle samples under a microscope to reveal SMA related changes, like grouped muscle fiber atrophy. However recent advances in testing and the discovery of SMA related mutations have changed diagnostic methods. Nowadays genetic testing is often the step in diagnosing suspected SMA cases. This process involves examining DNA for SMN1 gene mutations the cause of SMA. The presence of mutations or absence/deletion of SMN1 exon 7 confirms an SMA diagnosis. Genetic testing is now the preferred method for SMA due to its accuracy, invasiveness and efficiency. It allows for diagnosis and prompt implementation of management and treatment strategies for individuals, with SMA (111-113).

1.1.8. Genetic Diagnosis

Diagnosing SMA through testing is usually straightforward because specific genetic mutations linked to the condition are quite common. 95% of SMA patients exhibit deletions of exon 7 and 8 or just exon 7 in the SMN1 gene. Confirming mutations, in SMN1 helps establish a diagnosis of 5q SMA, which's the most prevalent form of SMA. Recent recommendations stress the significance of assessing both SMN2 copy numbers and SMN1 deletions for confirmation of SMA. Understanding SMN2 copy numbers offers insights into disease severity among patients and aids in identifying presymptomatic individuals who could benefit from early intervention. Various methods can be utilized to identify SMN1 deletions and determine SMN2 copy numbers, such as. Quantitative Real Time PCR: This method tracks DNA amplification in time. Is commonly employed for detecting SMN1 deletions and determining SMN2 copy numbers. Multiplex Ligation Dependent Probe Amplification (MLPA); Regarded as the gold standard, for determining SMN2 copy numbers MLPA uses probes to detect and measure the quantity of SMN2 copies. Digital PCR: Digital droplet PCR is a highly sensitive technique that enables precise quantification of DNA

copies, including determining SMN2 copy numbers. NGS (Next Generation Sequencing) techniques have been developed to determine the copy number of SMN2 showing outcomes. While MLPA is commonly used it has limitations when dealing with SMN2 copy numbers exceeding two. Different MLPA approaches may produce varying results underscoring the need, for reliability assessments and quality control measures in lab environments. Real time PCR and digital droplet PCR present alternative methods for quantification of SMN2 copy numbers. The genetic diagnosis of SMA involves evaluating both SMN1 deletions and SMN2 copy numbers, which can be assessed using methods with varying levels of precision and dependability. These genetic tests are vital, for confirming SMA diagnoses predicting disease severity and guiding treatment choices for individuals (111-113).

1.1.9. Other Diagnostic Tests for SMA

Apart, from tests there are diagnostic assessments and markers that doctors can use to evaluate and manage patients with SMA. Serum Creatine Kinase (CK) Levels; SMA patients might have serum CK levels, typically not surpassing 1,000 IU/l. However elevated CK levels could mistakenly suggest a muscle related cause for weakness. EMG testing can assist in distinguishing between causes of muscle weakness. Serum Creatinine Levels: Individuals with SMA type 1 or 2 often display reduced serum creatinine levels due to decreased muscle mass. Chest Radiography: In individuals with SMA type 1 chest X rays frequently reveal characteristics like a bell-shaped thorax and a rib deformity resembling a "parasol," which indicates weakened muscles but relatively preserved diaphragm function. Biomarkers: Helpful biomarkers such as nerve compound motor action amplitude and blood neurofilament levels can provide additional predictive insights and serve as indicators for treatment response. However, their use is currently limited to research settings, than clinical practice (114).

1.1.10. Screening

Various methods are used to screen for SMA such, as preconception carrier screening, prenatal testing and newborn screening. Before conception carrier screening

can identify individuals carrying a mutation in the SMN1 gene. This screening is important for couples regardless of their family history of SMA as SMN1 deletions are relatively common in the population. A positive carrier status should prompt testing of the individuals' partner or gamete donor and counseling. Prenatal testing of the fetus can be done through procedures like villus sampling, amniocentesis or possibly by extracting cells from maternal circulation. Although prenatal testing for SMA has become less frequent due to therapies it may gain importance if fetal therapy for SMA becomes possible. The introduction of screening for SMA has brought progress leading to a better understanding of SMA frequency early treatment initiation before symptoms appear improved knowledge on biomarker responses to treatment and insights into the economic effects of early intervention. Newborn screening programs, for SMA are being implemented in countries to aid in the detection and management of affected individuals (115-120).

1.1.11. Prevention

The results, from research studies like NURTURE and SPR1NT provide evidence supporting the importance of screening newborns for SMA on. Treating infants before they show symptoms can result in medical benefits. Here are some key discoveries from these studies. NURTURE Study: In this phase II trial, 25 presymptomatic infants with SMN1 mutations and two or three copies of SMN2 were treated with nusinersen after birth due to either screening or family history. None of the infants showed SMA symptoms at the start of treatment. Initial analysis revealed that all infants were alive and continually improving their motor skills. They achieved the milestone of sitting by 9 months old. A majority were able to walk independently by 18 months old. A few infants needed support, and most did not require long term ventilation. SPR1NT Gene Therapy Study; This study involved 29 infants who received onasemnogene abeparvovec treatment, including those with two or three copies of SMN2. All patients survived until assessment points with many reaching sitting and walking milestones at appropriate ages. These results demonstrate the effectiveness of gene therapy, in helping presymptomatic SMA infants reach stages. These studies together show that starting treatment, in babies with SMA before symptoms appear can bring

improvements in motor skills and decrease the need for breathing assistance. Screening programs for newborns can help identify babies early enabling intervention and better results. The effectiveness of medications such as nusinersen and onasemnogene abeparvovec in babies, without symptoms highlights the significance of screening for SMA to enhance patient outcomes and quality of life (121-126).

1.2. Loop-Mediated Isothermal Amplification

Loop-Mediated Isothermal Amplification uses 4 6 primers that are tailored to identify 6 8 regions of the target DNA ensuring amplification. A strand displacing DNA polymerase kicks off the synthesis process while two crafted primers create "loop" structures to aid in rounds of amplification by extending on the loops and attaching additional primers. The resulting DNA products are >20 kb). Contain multiple repeats of the short (80–250 bp) target sequence, linked together with single stranded loop sections, in long concatamers. Although these products might not be ideal for manipulation due to their length the extensive amplification of the target allows for detection methods. Real time fluorescence detection using intercalators or probes lateral flow tests and agarose gel detection are all directly compatible with LAMP reactions. The equipment required for LAMP typically involves maintaining a heat level at the desired reaction temperature and incorporating real time fluorescence as necessary for analysis. LAMP is a method of nucleic acid amplification that employs 4 6 primers designed to identify 6 8 areas, in the target DNA. It utilizes a strand DNA polymerase to kickstart synthesis. Additionally, two of these primers create loop structures that assist in rounds of amplification. The special way the primer is designed, and the loop structures help speed up and amplify the target DNA efficiently in temperature conditions (127).

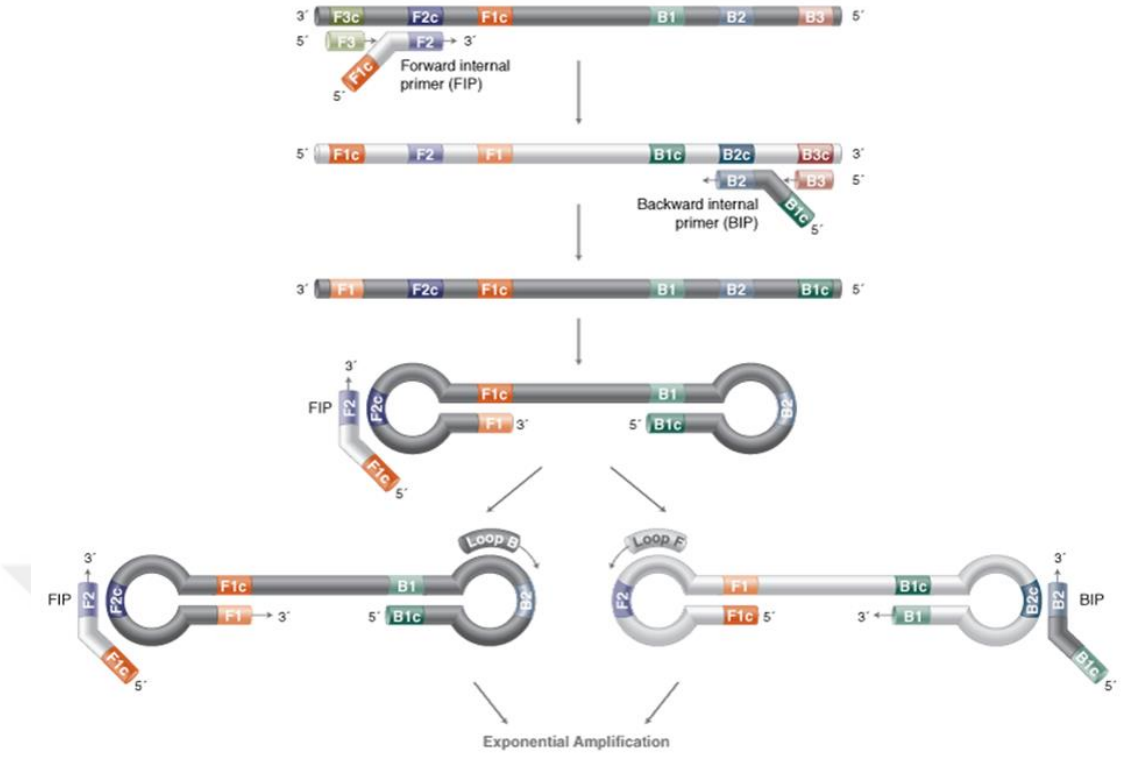

Figure 1 A diagram illustrating the Loop mediated amplification technique. The forward and backward primer attachment points, on the target DNA sequence, for LAMP **(128)**.

Loop-Mediated Isothermal Amplification is a technique, for amplifying genes that comes with benefits such as speed, ease of use and precision. The process involves amplifying DNA samples at a temperature of 60 °C – 65 °C by carrying out elongation reactions in loop regions within the target DNA sequence. These reactions include self-elongation of templates from the stem loop structure at the binding primers to the loop region. This continuous amplification leads to an increase in the target DNA amount in a short period. One notable advantage of LAMP is its straightforwardness, which is maintained across all stages from acid extraction to detection of amplification. It can be carried out using lab equipment without the need for thermal cycling devices since amplification occurs at a fixed temperature. Moreover, results are typically obtained within 30 minutes to an hour making LAMP a swift method for DNA amplification. The uncomplicated nature, quickness and specificity of the LAMP technique make it suitable for purposes such, as performing diagnoses of infectious diseases, genetic disorders, and other conditions at point of care settings. LAMP is an option, for use in

places with resources like developing nations, where access to advanced lab equipment and infrastructure might be scarce. It can help identify pathogens, impurities and genetic indicators in food and samples aiding in quality control and safety checks. LAMP provides an easy to use platform for amplifying DNA with potential uses in various fields such as medical testing, food safety and environmental surveillance. Its simplicity, speediness and accuracy make it a valuable tool for scientist's healthcare providers and industries, across sectors (129-133).

1.2.1. Molecular Mechanism of LAMP

Loop-Mediated Isothermal Amplification enhances the target DNA by utilizing a DNA polymerase, with activity and a set of four to six primers crafted for pinpointing regions within the target sequence. The amplification procedure involves a sequence of elongation reactions taking place at loop structures formed by the primers. The key elements of the reaction consist of the target DNA, DNA polymerase (*Bst* DNA polymerase) primers, deoxynucleotide triphosphates (dNTPs). Buffer to establish an optimal enzymatic setting. The process starts with denaturation, where the target DNA is split into strands followed by annealing, where the loop regions of the primers connect to sequences in the target DNA. Subsequently elongation happens as the DNA polymerase produces strands of DNA using the target sequence as a guide while displacing existing strands in the process. This cycle repeats itself resulting in an escalation in the amount of amplified target DNA. Detection of LAMP products can be accomplished through methods, like turbidity measurement, colorimetric indicators (e.g., SYBR Green) fluorescence or lateral flow devices (129-133).

1.2.2. Primer Design and Selection

Different types of primers utilized in LAMP consist of primers (FIP and BIP) which function as both reverse primers to kickstart DNA replication outer primers (F3 and B3) that act as both forward and reverse primers to amplify the DNA section and optional loop primers (LF and LB) that improve the speed and efficiency of amplification by targeting loop structures formed during the reaction. Factors

considered in primer design include specificity to ensure targeting of the desired DNA sequence melting temperatures (Tm), for effective annealing processes a length typically ranging from 18 to 25 nucleotides and the formation of loop structures with the target DNA for enhanced amplification efficiency. Primer design for LAMP tests can be carried out manually using tools like PrimerExplorer or Primer BLAST based on the target DNA sequence or predesigned primer sets are available from suppliers for sequences or pathogens. The LAMP system provides an approach for DNA amplification at a temperature with primer selection guided by design criteria allowing for manual creation or acquisition from commercial sources. This technique is widely applied across sectors such, as healthcare, agriculture and environmental monitoring (129-133).

1.3. Statistical Analysis

Sensitivity measures the probability that a test will correctly produce a positive result when the disease is present. It is also known as the true positive rate. A high sensitivity indicates that the test is effective in identifying individuals who have the disease (134).

Specificity measures the probability that a test will correctly produce a negative result when the disease is not present. This is referred to as the true negative rate. High specificity means the test is effective in ruling out individuals who do not have the disease (134).

The positive predictive value (PPV) represents the probability that an individual actually has the disease when the test result is positive. PPV provides insight into the likelihood that a positive test result accurately reflects the presence of the disease.

The negative predictive value (NPV) represents the probability that an individual does not have the disease when the test result is negative. NPV is important for understanding how effectively a negative test result can reassure that the disease is absent (135).

Accuracy measures the overall probability that the test correctly classifies individuals as either having or not having the disease. It combines the true positive and true negative results to provide an overall measure of test performance (136).

2. BACKGROUND AND AIM OF THE STUDY

When examining the research, on SMA disease and its preclinical models it becomes evident that patients experience a loss of motor neurons highlighting the importance of intervention. Moreover new drugs developed for treating this disease have shown increased effectiveness when administered on. Given these factors screening for SMA plays a role in fighting against the illness. The American College of Medical Genetics recommends SMA carrier status screening in the population with various countries conducting pilot studies on prenatal carrier testing (137). In the context of SMA disease key goals include identifying nucleotide changes and exome losses. DNA. Multiplex ligation dependent probe amplification methods serve as gold standards for these objectives (138). While these gold standard methods exist alongside techniques their widespread use is limited by factors such as time consumption, costliness, complex procedures/equipment requirements and the need for expert users. LAMP emerges as an efficient method that is increasingly being adopted. It delivers results within a 30 minute reaction time without requiring machinery like PCR due, to its single reaction temperature setting.

Due, to its sensitivity to inhibitors and the lack of a requirement for RNA/DNA isolation along with a preparation process this method can easily be used on samples. This field has seen advancements during the COVID 19. The incorporation of LAMP technology with probe systems ensures sensitivity in detecting mutations. The main goal of this project is to create a precise and cost effective screening/diagnostic method for SMA disease in comparison to current techniques utilizing the LAMP approach. The objective is to develop a kit that's more sensitive has a procedure than existing methods and can deliver quick results without the need, for sophisticated infrastructure.

3. MATERIALS AND METHODS

The workflow of the thesis methods which include primer design, optimization, validation, statistical analysis is visualized in Figure 2.

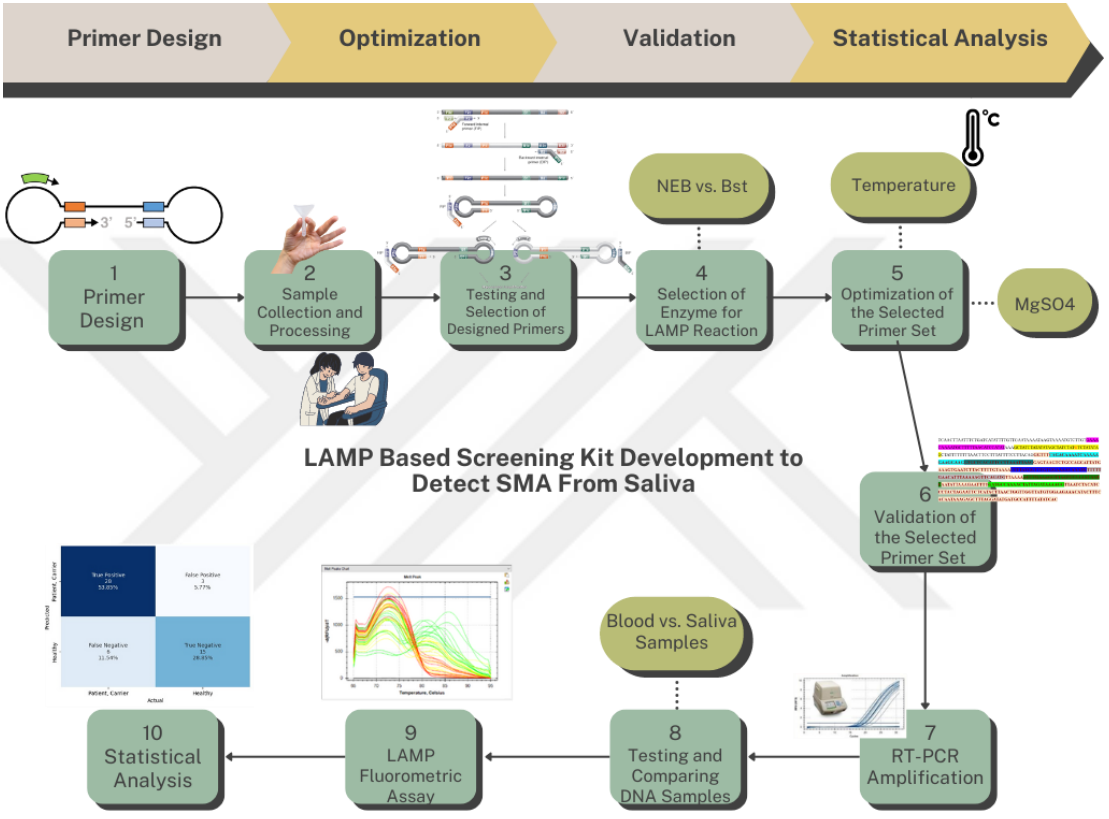

Figure 2 Visualization of the methods workflow

3.1. Primer Design

Three different LAMP primer sets were designed aiming to detect the SMN1:c.840C>T rs1164325688 variation and exon 7 deletion of human gene SMN1 sequence (UCSC Genome Browser RefSeq NM_000344). NEB® LAMP Primer Design Tool (available for free use at: https://lamp.neb.com/#!/) used for the first primer design. Na+ concentration, Mg++ concentration, primer lengths, Tm (min/max), GC content, ΔG threshold, distance between primer parameters were

changed in the Tool, and four different primers were automatically designed in the desired gene region in line with the parameters.

The second primer set was manually designed to match the targeted mutation. While performing manual design of six LAMP primers, heterodimer formation states, homodimer formation states, primer lengths, ΔG threshold, GC content, melting temperatures and hairpin Tm were taken into consideration.

The online software Primer Explorer V5 (available for free use at: https://primerexplorer.jp/e/) used for the third primer design. The sequence of the target gene was entered into the Primer Explorer V5 tool. Then, the parameters required for the design of six LAMP primers, including primer length, GC content, Tm values and the positions of the primers on the target gene, were determined. Primers with the desired properties were automatically designed with the tool.

3.2. Sample Collection and Processing

An ethics committee application was made for the research, the application was discussed at the Acıbadem Mehmet Ali Aydınlar University Medical Research Evaluation Board (ATADEK) meeting dated September 22, 2023, numbered 2023/14, and was found appropriate in terms of medical ethics with the decision number 2023-14/513 (ethics committee approval certificate is in Annex 1).

It was determined by statistical power analysis that the number of patients required to make statistical sense of the accuracy of the developed kit (determining that it had sensitivity and specificity values above 95%) was 18.

With the help of Assoc. Prof. Dr. Pınar Topaloğlu from Istanbul University - Çapa Hospital, saliva and blood samples of 18 patients, their mothers, fathers and siblings were taken in accordance with the rules of the Declaration of Helsinki.

For DNA isolation from blood and saliva samples taken from patients, ZYMO *Quick*-DNA™ Universal Kit (Cat. No.: D4069) was used in accordance with the instructions and the obtained DNA samples were stored at -20 °C. Contamination was checked and DNA amounts were measured with Thermo Scientific™ NanoDrop™ One Microvolume UV-Vis Spectrophotometer (Table 4).

3.3. Testing and Selection of Designed Primers

The first primer set was obtained at a concentration of 100 µM. Sufficient ddH_2O was added separately to the F3, B3, FIP, and BIP primers to prepare 200 µM stock primers. The concentrations of FIB – BIP and F3 – B3 in the primer mixture are 1.6 M and 0.4 M, respectively. To prepare the primer mixture, 1,25 µL of F3, 1,25 µL of B3, 10 µL of FIP, 10 µL of BIP, and 27,5 µL of ddH_2O were combined. For each sample reaction, 12,5 µL of WarmStart LAMP 2X Master Mix (E1700S), 0,5 µL of LAMP Fluorescent Dye, 1 µL of the prepared primer mixture, 9 µL of ddH_2O, and 2 µL of DNA sample were mixed and incubated on a real-time qPCR machine (BioRad CFX96) for 79 cycles at 65 °C. Melting curve analysis was performed between 65 °C and 95 °C, with measurements taken every 5 seconds and increasing by 0,5 °C.

The second and third primer sets were obtained at a concentration of 100 µM. Sufficient ddH_2O was added separately to the F3, B3, FIP, BIP, LoopF and LoopB primers to prepare 200 µM stock primers. The concentrations of FIB – BIP, F3 – B3, and LoopF – LoopB in the primer mixture are 1,6 M, 0,4 M, and 0,4 M, respectively. To prepare the primer mixture, 1 µL of F3, 1 µL of B3, 4 µL of FIP, 4 µL of BIP, 1

µL of LoopF, 1 µL LoopB and 8 µL of ddH_2O were combined. For each sample reaction, 12,5 µL of WarmStart LAMP 2X Master Mix (E1700S), 0,5 µL of LAMP Fluorescent Dye, 1 µL of the prepared primer mixture, 9 µL of ddH_2O, and 2 µL of DNA sample were mixed and incubated on a real-time qPCR machine (BioRad CFX96) for 79 cycles at 65 °C. Melting curve analysis was performed between 65 °C and 95 °C, with measurements taken every 5 seconds and increasing by 0,5 °C.

3.4. Selection of Enzyme for LAMP Reaction

For the NEB enzyme, the concentrations of FIB – BIP, F3 – B3, and LoopF – LoopB in the primer mixture are 1,6 M, 0,4 M, and 0,4 M, respectively. To prepare the primer mixture from second primer set, 1 µL of F3, 1 µL of B3, 4 µL of FIP, 4 µL of BIP, 1 µL of LoopF, 1 µL LoopB and 8 µL of ddH_2O were combined. For each sample reaction, 12,5 µL of WarmStart LAMP 2X Master Mix (E1700S), 0,5 µL of LAMP Fluorescent Dye, 1 µL of the prepared primer mixture, 9 µL of ddH_2O, and 2 µL of DNA sample were mixed and incubated on a real-time qPCR machine (BioRad CFX96) for 79 cycles at 62,5 °C. Melting curve analysis was performed between 62,5 °C and 95 °C, with measurements taken every 5 seconds and increasing by 0,5 °C.

For the Bioline *Bst* enzyme, the concentrations of FIB – BIP, F3 – B3, and LoopF – LoopB in the primer mixture are 1,6 M, 0,4 M, and 0,4 M, respectively. To prepare the primer mixture from second primer set, 1 µL of F3, 1 µL of B3, 4 µL of FIP, 4 µL of BIP, 1 µL of LoopF, 1 µL LoopB and 8 µL of ddH_2O were combined. For each sample reaction, 1 µL of *Bst* DNA Polymerase (8,000 U / ml) (M0275L), 13,25 µL of ddH_2O, 5 µL of Dntp mix (10 mM), 1,25 µL of EvaGreen dye, 1 µL of the prepared primer mixture, 2,5 µL of *Bst* Reaction Buffer (10X Thermopol Buffer) and 2 µL of DNA sample were mixed and incubated on a real-time qPCR machine (BioRad CFX96) for 79 cycles at 62 °C. Melting curve analysis was performed between 62 °C and 95 °C, with measurements taken every 5 seconds and increasing by 0,5 °C.

3.5. Optimization of the Selected Primer Set

3.5.1. Temperature Optimization

The temperature optimization of the selected *Bst* enzyme was conducted at temperatures of 70 °C, 69,6 °C, 68,8 °C, 67,4, 65,7, 64,4 °C, 62 °C, 60 °C, and 58 °C, 55,9 °C, 54 °C, 52 °C, 50 °C. The steps in Method 3.4 the steps for *Bst* enzyme reaction were repeated for all selected temperatures.

3.5.2. $MgSO_4$ Concentration Optimization

The primer mixture was prepared as described in Method 3.4, the steps for *Bst* enzyme reaction. The $MgSO_4$ concentration has been reduced by approximately 30% compared to previous reactions (1,5 µL (10 mM). For each sample reaction, 1 µL of *Bst* DNA Polymerase (8,000 U / ml) (M0275L), 11,25 µL of ddH_2O, 5 µL of dNTP, 1,25 µL of EvaGreen dye, 1 µL of the prepared primer mixture, 2,5 µL of *Bst* Reaction Buffer (10 X Thermopol Buffer), 1 µL $MgSO_4$ (100 mM) and 2 µL of DNA sample were mixed and incubated on a real-time qPCR machine (BioRad CFX96) for 79 cycles at 64,4 °C. Melting curve analysis was performed between 64,4 °C and 95 °C, with measurements taken every 5 seconds and increasing by 0,5 °C.

The same processes were repeated to increase $MgSO_4$ by approximately 30%. The amount of MgSO4 (100 mM) was changed to 1.5 µL while everything else in the reaction remained constant.

3.6. Validation of the Selected Primer Set

3.6.1. Validation of Primer Pairs via RT-PCR Amplification

The RT-PCR amplification was performed using the Zymo Tag polymerase enzyme with the primer pairs F3 – B3, FIP – BIP, F3 – LoopF, and B3 - LoopB. The 10 mM primer mixture was prepared by adding 38 µL of ddH_2O to 2 µL of each: F3, B3, FIP, BIP, LoopF, and LoopB. Pairs of forward and reverse primers were grouped in sets of two for the RT-PCR reaction. Each set consisted of 0,5 µL F3 + 0,5 µL B3, 0,5 µL FIP + 0,5 µL BIP, 0,5 µL F3 + 0,5 µL LoopF, and 0,5 µL B3 + 0,5 µL LoopB. All of these sets were individually tested for the same samples. In the reaction mixture, 12,5 µL of Zymo Tag qPCR Premix (E2054), 2,5 µL of primer forward, 2,5 µL of primer reverse, 7,5 µL of ddH_2O, and 2 µL of DNA sample were mixed for each sample and incubated on a real-time qPCR machine (BioRad CFX96). The reaction template underwent a denaturation step at 95 °C for 10 minutes, followed by a 35 cycle amplification step consisting of denaturation at 95 °C for 30 seconds, annealing at 50 °C for 30 seconds, and extension at 68 °C for 1 minute and 30 seconds. Finally, the reaction was completed with a final extension at 68 °C for 10 minutes and cooling to 4 °C.

3.6.2. Testing and Comparing DNA Samples Obtained from Blood and Saliva

For the LAMP reaction with *Bst* enzyme and second primer set, the concentrations of FIB – BIP, F3 – B3, and LoopF – LoopB in the primer mixture are 1,6 M, 0,4 M, and 0,4 M, respectively. To prepare the primer mixture from second primer set, 2 µL of F3, 2 µL of B3, 8 µL of FIP, 8 µL of BIP, 2 µL of LoopF, 2 µL LoopB and 16 µL of ddH_2O were combined. For each sample reaction, 1 µL of *Bst* DNA Polymerase (8,000 U / ml) (M0275L), 13,25 µL of ddH_2O, 5 µL of Dntp mix (10 mM), 1.25 µL of EvaGreen dye, 1 µL of the prepared primer mixture, 2,5 µL of *Bst* Reaction Buffer (10X Thermopol Buffer) and 2 µL of DNA sample were mixed and incubated on a real-time qPCR machine (BioRad CFX96) for 79 cycles at 64,4 °C. Melting curve analysis was performed between 65 °C and 95 °C, with measurements taken every 5

seconds and increasing by 0,5 °C.

3.6.3. RT LAMP Fluorometric Assay with Patient, Carrier, and Positive Controls

For the LAMP reaction with *Bst* enzyme and second primer set, the concentrations of FIB – BIP, F3 – B3, and LoopF – LoopB in the primer mixture are 1,6 M, 0,4 M, and 0,4 M, respectively. To prepare the primer mixture from second primer set, 2 µL of F3, 2 µL of B3, 8 µL of FIP, 8 µL of BIP, 2 µL of LoopF, 2 µL LoopB and 16 µL of ddH_2O were combined. For each sample reaction, 1 µL of *Bst* DNA Polymerase (8,000 U / ml) (M0275L), 13,25 µL of ddH_2O, 5 µL of Dntp mix (10 mM), 1,25 µL of EvaGreen dye, 1 µL of the prepared primer mixture, 2,5 µL of *Bst* Reaction Buffer (10X Thermopol Buffer) and 2 µL of DNA sample were mixed and incubated on a real-time qPCR machine (BioRad CFX96) for 79 cycles at 64,4 °C. Melting curve analysis was performed between 65 °C and 95 °C, with measurements taken every 5 seconds and increasing by 0,5 °C. (The same steps were repeated within 3 trials.)

The workflow of LAMP-based SMA test which include sample collection, sample preparation, sample amplification, sample detection is visualized in Figure 3.

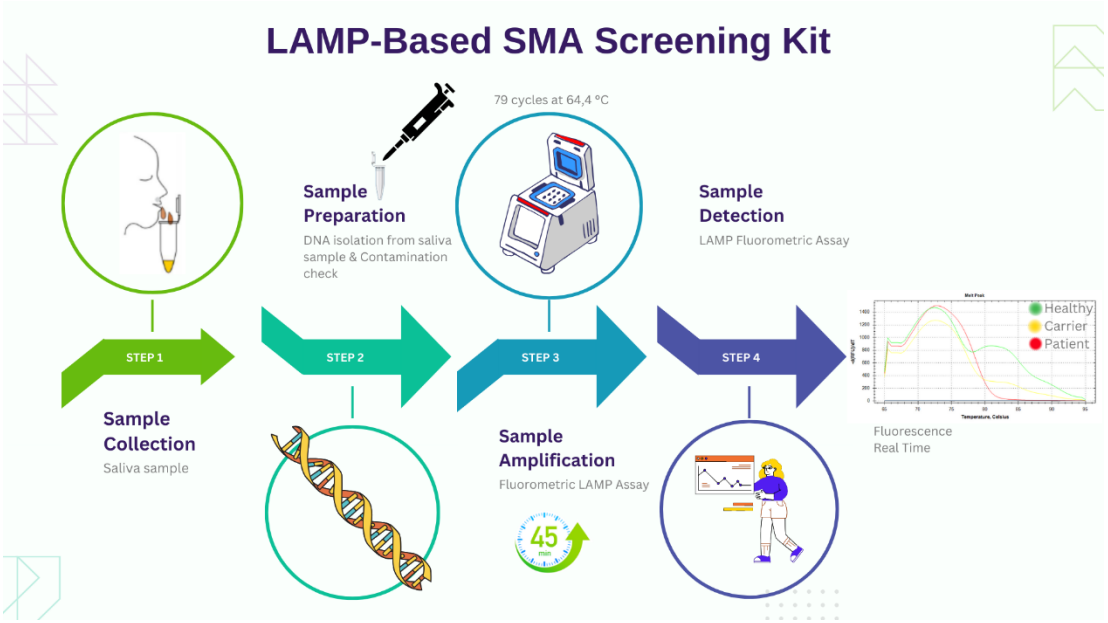

Figure 3 Visualization of LAMP-based SMA test workflow

3.7. Statistical Calculation

$$Sensitivity = \frac{TP}{TP + FN}$$

$$Specificity = \frac{TN}{FP + TN}$$

$$PPV = \frac{sensitivity \times prevalence}{sensitivity \times prevalence + (1 - specificity) \times (1 - prevalence)}$$

$$NPV = \frac{specificity \times (1 - prevalence)}{(1 - sensitivity) \times prevalence + specificity \times (1 - prevalence)}$$

$$Accuracy = Sensitivity \times Prevalence + Specificity \times (1 - Prevalence)$$

Statistical calculations were made using the above derivations.

4. RESULTS

4.1. Primer Design

Positions of first primer set's primers (F1, F2, F3, B1, B2, B3) (Figure 4) designed with NEB® LAMP Primer Design Tool on the target gene region taken from the UCSC Genome browser. The C nucleotide shown in red (Figure 4) indicates the position where the mutation of interest occurs. The primers were designed at the ends of certain primers specifically for the allele to identify this mutation.

TCAACTTAATTTCTGATCATATTTTGTTGAATAAAATAAGTAAAATGTCTTGTGAAA
CAAAATGCTTTTTAACATCCATATAAAGCTATCTATATATAGCTATCTATGTCTATATA
GCTATTTTTTTTAACTTCCTTTATTTTCCTTACAGGGTTTCAGACAAAATCAAAAA
GAAGGAAGGTGCTCACATTCCTTAAATTAAGGAGTAAGTCTGCCAGCATTATG
AAAGTGAATCTTACTTTTGTAAAACTTTATGGTTTGTGGAAAACAAATGTTTTT
GAACATTTAAAAAGTTCAGATGTTAAAAAGTTGAAAGGTTAATGTAAAACAAT
CAATATTAAAGAATTTTGATGCCAAAACTATTAGATAAAAGGTTAATCTACATC
CCTACTAGAATTCTCATACTTAACTGGTTGGTTATGTGGAAGAAACATACTTTC
ACAATAAAGAGCTTTAGGATATGATGCCATTTTATATCAC

Figure 4 The locations of the first primer set's primers are shown in exon 7 of the SMN1 gene.

Primer designs with positions from 5' to 3' of the DNA are in Table 1. Primers to be used in the reaction were obtained: F3 primer, B3 primer, FIP: F1 complementary + F2, BIP: B2 + B1 complementary.

Table 1 First Primer Set

LAMP Primer	Sequence (5'---► 3')
F3	CGGTCCAATGCTTTTTAACATCCATAGGTCCG
B3	GCTGCCTTTAGGATATGATGCCATTTGCTGCG
FIP	GCGCGAAACCCTGTAAGGAAAATAGCTTTTG
	CTCTATATATAGCTATCTATG
BIP	GCGCAAACATACTTTCACAATAAATTTTCCAC
	ATAACCAACCAGTTAAGTATGA

Positions of second primer set's primers (F1, F2, F3, B1, B2, B3) (Figure 5) designed with manually on the target gene region taken from the UCSC Genome browser. The C nucleotide shown in red (Figure 5) indicates the position where the mutation of interest occurs. The primers were designed at the ends of certain primers specifically for the allele to identify this mutation.

TCAACTTAATTTCTGATCATATTTTGTTGAATAAAATAAGTAAAATGTCTTGTGAAA
CAAAATGCTTTTTAACATCCATATAAAGCTATCTATATATAGCTATCTATGTCTATATA
GCTATTTTTTTTAACTTCCTTTATTTTCCTTACAGGGTTTCAGACAAAATCAAAAA
GAAGGAAGGTGCTCACATTCCTTAAATTAAGGAGTAAGTCTGCCAGCATTATG
AAAGTGAATCTTACTTTTGTAAAACTTTATGGTTTGTGGAAAACAAATGTTTTT
GAACATTTAAAAAGTTCAGATGTTAAAAAGTTGAAAGGTTAATGTAAAACAAT
CAATATTAAAGAATTTTGATGCCAAAACTATTAGATAAAAGGTTAATCTACATC
CCTACTAGAATTCTCATACTTAACTGGTTGGTTATGTGGAAGAAACATACTTTC
ACAATAAAGAGCTTTAGGATATGATGCCATTTTATATCAC

Figure 5 The locations of the second primer set's primers are shown in exon 7 of the SMN1 gene.

Primer designs with positions from 5' to 3' of the DNA are in Table 2. As explained in Figure 1 primers to be used in the reaction were obtained: F3, B3 complementary, LoopF complementary is between F1 and F2, LoopB is between B1 and B2, FIP: F1 complementary + F2, BIP: B1 + B2 complementary. While designing

the second primer set, care was taken to ensure that the targeted mutation was in the LoopF primer (Table 2).

Table 2 Second Primer Set

LAMP Primer	Sequence (5'---► 3')
F3	**GAAACAAAATGCTTTTTAACATCCATAT**
B3	**CCTTTTATCTAATAGTTTTGGCATC**
LOOP F	**CTTCCTTCTTTTTGATTTTGTCTG**
LOOP B	**TTTTTGAACATTTAAAAAGTTCAGATG**
FIP	**CTTAATTTAAGGAATGTGAGCACTTTT GCTATCTATATATAGCTATCTATGTCTATATAG**
BIP	**CTTTATGGTTTGTGGAAAACAAATGTTTTGATT GTTTTACATTAACCTTTCAACT**

Positions of third primer set's primers (F1, F2, F3, B1, B2, B3) (Figure 6) designed with the online software Primer Explorer V5 on the target gene region taken from the UCSC Genome browser. The C nucleotide shown in red (Figure 6) indicates the position where the mutation of interest occurs. The primers were designed at the ends of certain primers specifically for the allele to identify this mutation.

CCCCCTACCTCCGCCTCCCAAAGTTGTGGGATTGTAGGCATGAGCCACTGCAAGAA
AACCTTAACTGCAGCCTAATAATTGTTTTCTTTGGGATAACTTTTAAAGTACATTAA
AAGACTATCAACTTAATTTCTGATCATATTTTGTTGAATAAAATAAGTAAAATGTCTT
GTGAAACAAAATGCTTTTTAACATCCATATAAAGCTATCTATATATAGCTATCTATGT
CTATATAGCTATTTTTTTTAACTTCCTTTATTTTCCTTACAGGGTTTCAGACAAAATC
AAAAAGAAGGAAGGTGCTCACATTCCTTAAATTAAGGAGTAAGTCTGCCAGC
ATTATGAAAGTGAATCTTACTTTTGTAAAACTTTATGGTTTGTGGAAAACAAAT
GTTTTTGAACATTTAAAAAGTTCAGATGTTAAAAAGTTGAAAGGTTAATGTAA
AACAATCAATATTAAAGAATTTTGATGCCAAAAC

Figure 6 The locations of the third primer set's primers are shown in exon 7 of the SMN1 gene.

Primer designs with positions from 5’ to 3’ of the DNA are in Table 3. Primers to be used in the reaction were obtained: F3, B3 complementary, LoopF complementary is between F1 and F2, LoopB is between B1 and B2, FIP: F1 complementary + F2, BIP: B1 + B2 complementary. While designing the third primer set, care was taken to ensure that the targeted mutation was in the BIP primer (Table 3).

Table 3 Third Primer Set

LAMP Primer	Sequence (5’---► 3’)
F3	CATTAAAAGACTATCAACTTAATTTCTG
B3	**AAAAGTAAGATTCACTTTCATAATGC**
LOOP F	ATGTTAAAAAGCATTTTGTTTCAC
LOOP B	**AGACAAAATCAAAAAGAAGGAAGG**
FIP	CATAGATAGCTATATATAGATAGCTT TATATGGTTTTCATATTTTGTTGAATA AAATAAGTAAAATGTC
BIP	**TTAACTTCCTTTATTTTCCTTACAGG GTTTC**TTTTGGCAGACTTACTCCTTAA TTTAA

4.1.1. First Primer Set

Melting temperature values of the primers in the first LAMP primer set were between 60 ºC and 65 ºC as desired (Table 4). The blue sequences (Table 4) are sequences added to increase the stability of primers not found in the SMN1 gene.

Table 4 The first primer set includes the primers F3, B3, FIP and BIP along with their lengths, GC percentages, melting temperatures, and hairpin temperatures.

	Sequence	Length	GC Content	Melt Temp	Hairpin T_m (ºC)
F3	CGGTCCAATGCTTTTTAACATCC ATAGGTCCG	32	46,9 %	62,1 ºC	31,5
B3	GCTGCCTTTAGGATATGATGCC ATTTGCTGCG	32	50 %	64,2 ºC	39,8
FIP	GCGCGAAACCCTGTAAGGAAA ATAGCTTTTGCTCTATATATAG CTATCTATG	52	38,5 %	64,1 ºC	44,6
BIP	GCGCAAACATACTTTCACAAT AAATTTTCCACATAACCAACC AGTTAAGTATGA	54	33,3 %	64,4 ºC	37,8

When looking at the hetero-dimer and self-dimer stability of the primers in the first LAMP primer set, FIP's self-dimer stability and FIP-BIP hetero-dimer stability have the lowest Delta G value. BIP's self-dimer stability is also slightly below normal. Hetero-dimer and self-dimer stability of other primers is at normal values. (Table 5)

Table 5 The Delta G (kcal/mol) values for hetero-dimer and self-dimer stability of the primers F3, B3, FIP and BIP in the first primer set.

	F3	B3	FIP	BIP
F3	-6.68 kcal/mol	-6.12 kcal/mol	-5.99 kcal/mol	-6.19 kcal/mol
B3		-4.67 kcal/mol	-6.75 kcal/mol	-8.98 kcal/mol
FIP			-11.46 kcal/mol	-11.95 kcal/mol
BIP				-9.89 kcal/mol

4.1.2. Second Primer Set

In the second primer set, the spinning temperatures of the primers were determined to be minimum approximately 50 °C (Table 6). The blue sequences in FIP and BIP primers (Table 6) are sequences added to increase the stability of primers not found in the SMN1 gene. GC content, hairpin Tm and length values of the primers in the second primer set are suitable for the LAMP system. (Table 6)

Table 6 The lengths, GC percentages, melting temperatures, and hairpin temperatures of the primers F3, B3, FIP, BIP, LoopF and LoopB in the second primer set are listed.

	Sequence	Length	GC Content	Melt Temp	Hairpin T_m (ºC)
F3	GAAACAAAATGCTTTTTAACAT CCATAT	28	25 %	52 ºC	29,2
B3	CCTTTTATCTAATAGTTTTGGCA TC	25	32 %	50,3 ºC	14,3
LoopF	CTTCCTTCTTTTTGATTTTGTCTG	24	33,3 %	50,9 ºC	22,7
LoopB	TTTTTGAACATTTAAAAAGTTCA GATG	27	22,2 %	50,1 ºC	41,2
FIP	CTTAATTTAAGGAATGTGAGCA CTTTTGCTATCTATATATAGCTA TCTATGTCTATATAG	60	28,3 %	61,1 ºC	38
BIP	CTTTATGGTTTGTGGAAAACAA ATGTTTTGATTGTTTTACATTAA CCTTTCAACT	55	27,3 %	63 ºC	47,5

The stability of the possible dimers that the primers could form each other and with themselves was examined (Table 7). Due to the length of FIB and BIP primers (Table 7), the stability of possible self and heterodimers is high. The hetero-dimer and self-dimer stability of the primers in the second LAMP primer set LoopB-F3 hetero-dimer stability have the lowest Delta G value. Hetero-dimer and self-dimer stability of other primers was at normal values (Table 7).

Table 7 The Delta G (kcal/mol) values for hetero-dimer and self-dimer stability of the primers F3, B3, FIP, BIP, LoopF and LoopB in the second primer set.

	F3	B3	LoopF	LoopB	FIP	BIP
F3	-5.83 kcal/mol	-7.79 kcal/mol	-10.6 kcal/mol	-12.28 kcal/mol	-7.79 kcal/mol	-9.13 kcal/mol
B3		-3.14 kcal/mol	-3.42 kcal/mol	-7.43 kcal/mol	-6.61 kcal/mol	-7.18 kcal/mol
LoopF			-1.57 kcal/mol	-9.38 kcal/mol	-10.13 kcal/mol	-7.18 kcal/mol
LoopB				-8.74 kcal/mol	-8.77 kcal/mol	-10.6 kcal/mol
FIP					-11.46 kcal/mol	-6.71 kcal/mol
BIP						-11.07 kcal/mol

4.1.3. Third Primer Set

In the third primer set, the spinning temperatures of the primers were determined to be minimum approximately 50 °C (Table 8). The blue sequences in FIP and BIP primers (Table 8) are sequences added to increase the stability of primers not found in the SMN1 gene. GC content, hairpin Tm and length values of the primers in the third primer set are suitable for the LAMP system. (Table 8)

Table 8 The lengths, GC percentages, melting temperatures, and hairpin temperatures of the primers F3, B3, FIP, BIP, LoopF and LoopB in the third primer set are listed.

	Sequence	Length	GC Content	Melt Temp	Hairpin T_m (ºC)
F3	CATTAAAAGACTATCAACTTAATTTCTG	28	25 %	49,5 ºC	20,8
B3	AAAAGTAAGATTCACTTTCATAATGC	26	26,9 %	50,6 ºC	34,5
LoopF	ATGTTAAAAAGCATTTTGTTTCAC	24	25 %	49,6 ºC	36,9
LoopB	AGACAAAATCAAAAAGAAGGAAGG	24	33,3 %	51,9 ºC	26,8
FIP	CATAGATAGCTATATATAGATAGCTTTATATGGTTTTCATATTTTGTTGAATAAAATAAGTAAAATGTC	69	21,7 %	61,2 ºC	45,8
BIP	TTAACTTCCTTTATTTTCCTTACAGGGTTTCTTTTGGCAGACTTACTCCTTAATTTAA	58	31 %	64,2 ºC	35,3

The stability of the possible dimers that the primers could form each other and with themselves was examined (Table 9). Due to the length of FIB and BIP primers (Table 9), the stability of possible selfdimers and heterodimers is high. The hetero-dimer and self-dimer stability of the primers in the third LAMP primer set LoopB-BIP hetero-dimer stability have the lowest Delta G value. Hetero-dimer and self-dimer stability of other primers was at normal values without LoopF-LoopB heterodimer. (Table 9).

Table 9 The Delta G (kcal/mol) values for hetero-dimer and self-dimer stability of the primers F3, B3, FIP, BIP, LoopF and LoopB in the third primer set.

	F3	B3	LoopF	LoopB	FIP	BIP
F3	-6.32 kcal/mol	-6.33 kcal/mol	-5.83 kcal/mol	-5.36 kcal/mol	-6.82 kcal/mol	-9.01 kcal/mol
B3		-6.83 kcal/mol	-8.51 kcal/mol	-5.49 kcal/mol	-6.95 kcal/mol	-7.44 kcal/mol
LoopF			-5.83 kcal/mol	-10.6 kcal/mol	-9.26 kcal/mol	-7.43 kcal/mol
LoopB				-1.57 kcal/mol	-10.6 kcal/mol	-11.73 kcal/mol
FIP					-11.46 kcal/mol	-10.21 kcal/mol
BIP						-5.36 kcal/mol

4.2. Sample Collection and Processing

According to the NanoDrop measurement results of DNA obtained from blood and saliva samples, in the box plot, the median nucleic acid concentration for blood samples is approximately 40 ng/µL, with some outliers observed. For saliva samples, the median concentration is around 50 ng/µL, and there is also one outlier in this group. Overall, saliva samples appear to have a slightly higher nucleic acid concentration compared to blood samples. The box plot illustrates the variation in measurements, showing the minimum, maximum, and quartile values for each sample type (Figure 7). The A260/A280 ratio is a measure of DNA purity, with a value of approximately 1.8 indicating optimal purity. In this plot, the median A260/A280 ratio for both blood and saliva samples is close to 1.8, suggesting good DNA purity across both sample types. There are a few outliers observed in both groups, with one outlier below 1.8 in the blood samples and one outlier above 2.0 in the saliva samples. The plot also shows the variation in the ratios, displaying the minimum, maximum, and quartile values for each

sample type. Overall, both blood and saliva samples demonstrate similar levels of DNA purity based on the A260/A280 ratio.

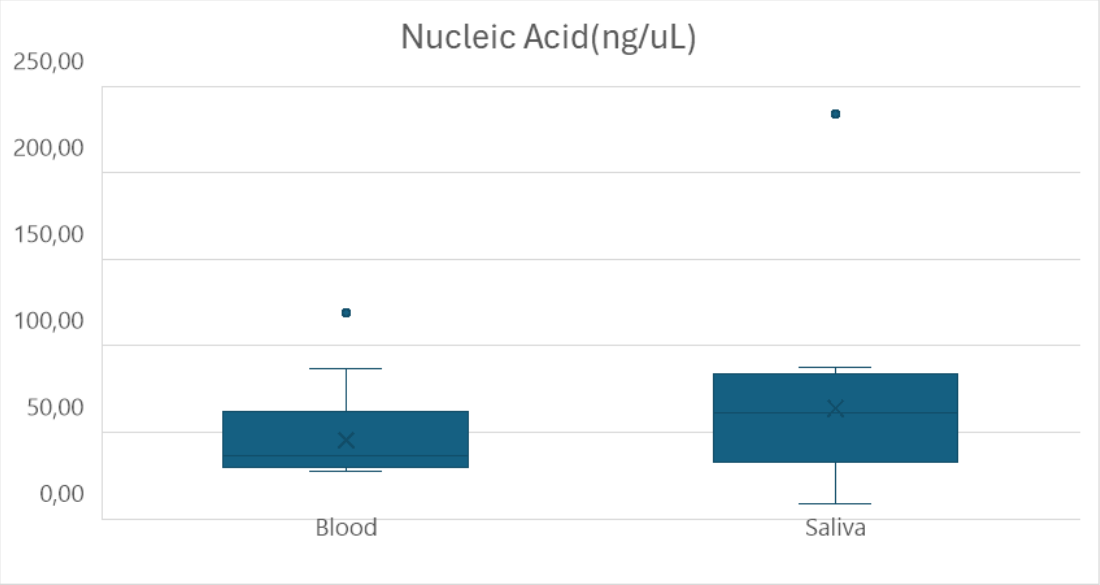

Figure 7 Box plot comparing nucleic acid concentrations (in ng/µL) between blood and saliva samples.

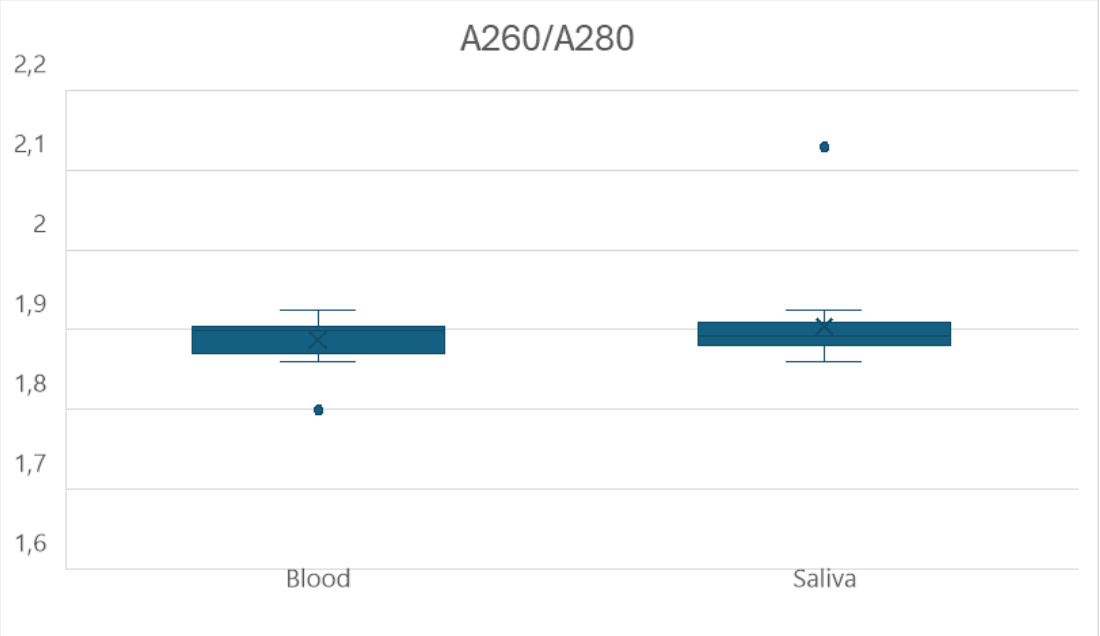

Figure 8 Box plot comparing the A260/A280 ratios of DNA obtained from blood and saliva samples.

4.3. Testing and Selection of Designed Primers

Real Time LAMP analyzes were performed to select the most suitable one of the 3 different designed LAMP primers. SMN1:c.840C>T rs1164325688 variation has been associated with SMA disease in the literature, screening for SMA disease is performed according to the homozygosity and heterozygosity status of this variation. This mutation is in the FIP primer in the first and third primer sets, and in the LoopF primer in the second primer set. Since the possible mutation point in the BIP and LoopF primers will affect the amplification in patients and carriers, in LAMP results, little or no amplification is expected in SMA patients (since the primer cannot be connected to the mutation point), and 50% less amplification (heterozygosity status of this variation) is expected in carriers than in healthy individuals. In healthy individuals, since there is no mutation, it is expected that all primers will bind target gene region and amplification will be maximum. Samples of healthy individuals who were sure to not have the targeted mutation and exon deletion were used as positive controls in the research.

As a result of RT LAMP performed with the first primer set, samples of patients, carriers and healthy individuals did not show any significant difference from each other (Figure 9) Therefore, the first primer set was not used in further optimization experiments.

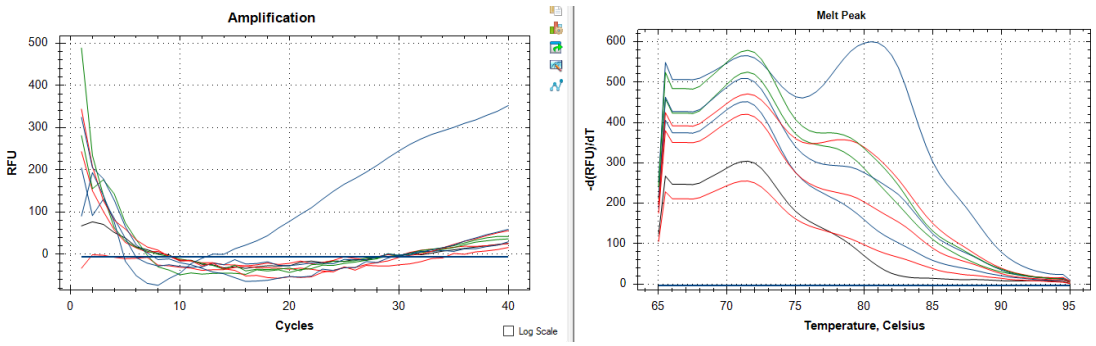

Figure 9 Result of testing and selection of first primer set. The amplification plot of the first LAMP primer set is shown as a line graph of relative fluorescence units (RFU) values versus cycles (left). The melting curve peak points of the first LAMP primer set are shown as a line graph of the time-dependent derivative of relative fluorescence units (-d(RFU)/dT) values versus temperatures (right). The samples represented by red, blue, green and black respectively indicate patients, carriers, healthy and blank solution.

In the RT LAMP results of the second primer set, there is a significant increase between 80 °C and 85 °C in the curve peak graph in the samples of carrier individuals compared to the samples of patient individuals (for individuals with the targeted mutation) (Figure 10). As a result of RT LAMP performed with the third primer set, there was no increase in the curve peak graph in carrier individuals compared to patient individuals between 80 °C and 85 °C. At the same time, contrary to expectations, amplification was observed in the negative control, which is the blank solution. Therefore, the third primer set was not used in further optimization experiments (Figure 11). Based on all these results, it was decided to use the second primer set in all other optimization experiments.

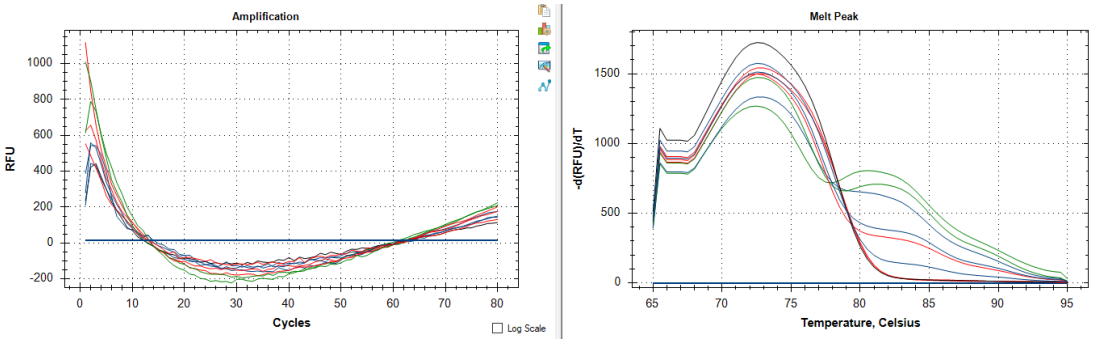

Figure 10 Result of testing and selection of second primer sets. The amplification plot of the second LAMP primer set is shown as a line graph of relative fluorescence units (RFU) values versus cycles (left). The melting curve peak points of the second LAMP primer set are shown as a line graph of the time-dependent derivative of relative fluorescence units (-d(RFU)/dT) values versus temperatures (right). The samples represented by red, blue, green and black respectively indicate patients, carriers, healthy and blank solution.

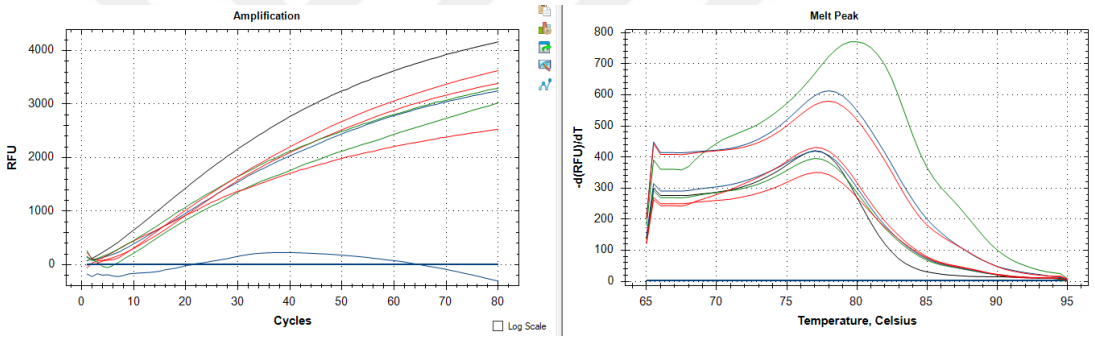

Figure 11 Result of testing and selection of third primer sets. The amplification plot of the third LAMP primer set is shown as a line graph of relative fluorescence units (RFU) values versus cycles (left). The melting curve peak points of the third LAMP primer set are shown as a line graph of the time-dependent derivative of relative fluorescence units (-d(RFU)/dT) values versus temperatures (right). The samples represented by red, blue, green and black respectively indicate patients, carriers, healthy and blank solution.

4.4. Selection of Enzyme for LAMP Reaction

Since the Bioline *Bst* enzyme accurately distinguishes patients and carriers, the *Bst* enzyme will continue to be used in future stages. In addition, in the experiment performed with Bioline *Bst* enzyme, samples of healthy individuals and samples of patient individuals are separated from each other by a significant difference in the peak curve graph. As expected, the positive control (healthy individuals) has the highest

derivation, while carriers have a lower derivation, and samples from patients have the lowest derivation value, even close to 0. (Figure 13). However, contrary to expectations, in the experiment with NEB enzyme, the positive control has almost the same level of derivation (-d(RFU)/dT) as patients and lower derivation than carriers (Figure 12).

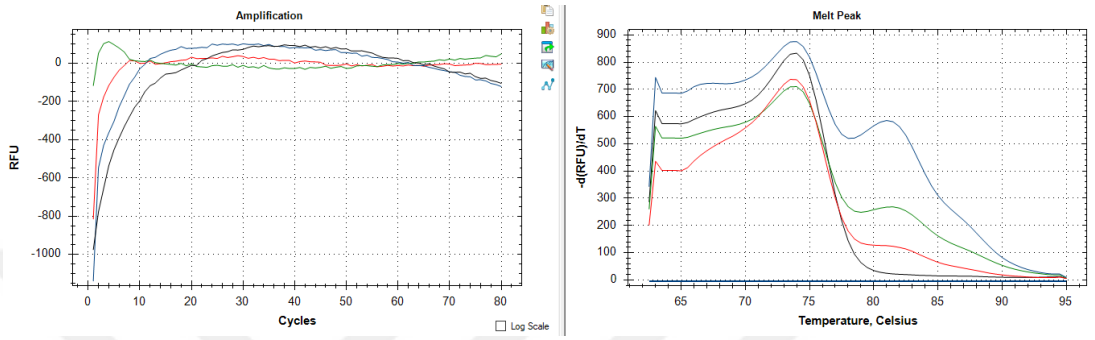

Figure 12 NEB enzyme was used in enzyme selection experiments for the LAMP reaction. The amplification plot of the NEB enzyme is shown as a line graph of relative fluorescence units (RFU) values versus cycles (left). The melting curve peak points of the NEB enzyme are shown as a line graph of the time-dependent derivative of relative fluorescence units (-d(RFU)/dT) values versus temperatures (right). The samples represented by red, blue, green and black respectively indicate patients, carriers, healthy and blank solution.

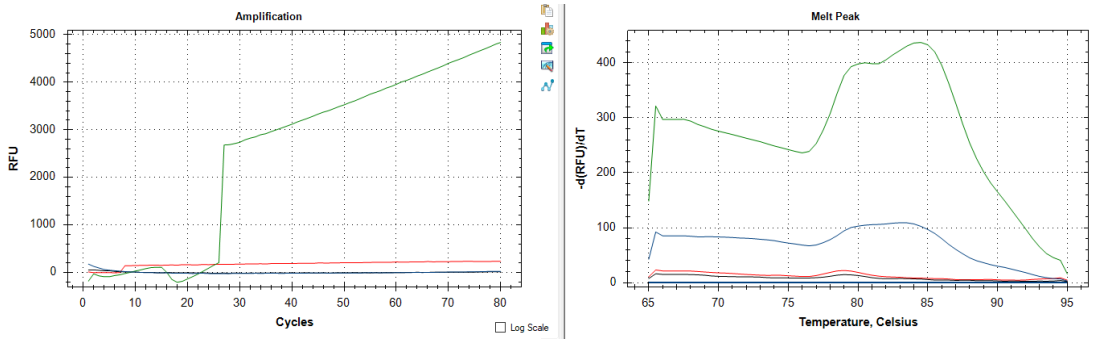

Figure 13 Bioline *Bst* enzyme was used in enzyme selection experiments for the LAMP reaction. The amplification plot of the *Bst* enzyme is shown as a line graph of relative fluorescence units (RFU) values versus cycles (left). The melting curve peak points (melt peak) of the *Bst* enzyme are shown as a line graph of the time-dependent derivative of relative fluorescence units (-d(RFU)/dT) values versus temperatures (right). The samples represented by red, blue, green and black respectively indicate patients, carriers, healthy and blank solution.

4.5. Optimization of the Selected Primer Set

4.5.1. Temperature Optimization

Real Time LAMP analyzes were performed at different temperatures between 50 °C and 70 °C to find the temperature value would best distinguish the samples of patients, carriers and healthy individuals from each other by using the *Bst* enzyme, which was determined to be more suitable for the LAMP reaction.

It was observed that the values of 70 °C, 69,6 °C, 68,8 °C, 67,4 °C, 65,7 °C were high temperatures for the LAMP system, and contrary to expectations, there was an increase in the amplification curve even in the blank solution and samples of patients individuals. In addition, samples of carriers, patients and healthy individuals could not be distinguished from each other. (Figure 14 – Figure 18).

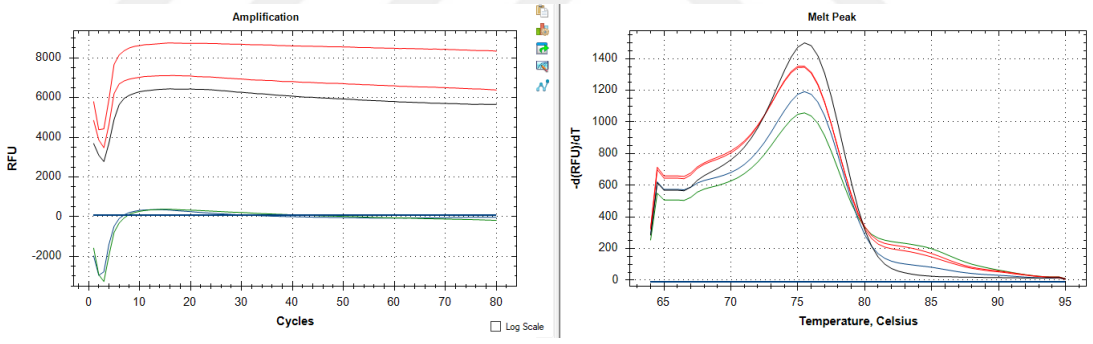

Figure 14 The result of trying 70 °C in temperature optimization. The amplification plot at 70°C is shown as a line graph of relative fluorescence units (RFU) values versus cycles (left). The melting curve peak points at 70°C are shown as a line graph of the time-dependent derivative of relative fluorescence units (-d(RFU)/dT) values versus temperatures (right). The samples represented by red, blue, green and black respectively indicate patients, carriers, healthy and blank solution.

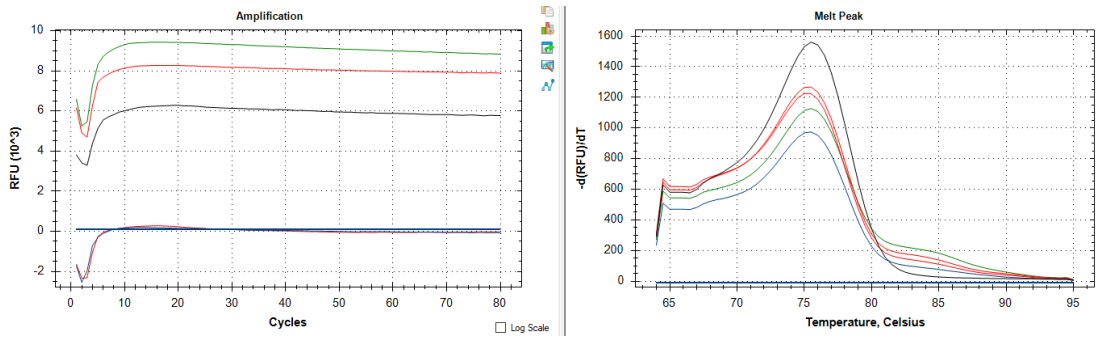

Figure 15 The result of trying 69,6 °C in temperature optimization. The amplification plot at 69,6 °C is shown as a line graph of relative fluorescence units (RFU) values versus cycles (left). The melting curve peak points at 69,6 °C are shown as a line graph of the time-dependent derivative of relative fluorescence units (-d(RFU)/dT) values versus temperatures (right). The samples represented by red, blue, green and black respectively indicate patients, carriers, healthy and blank solution.

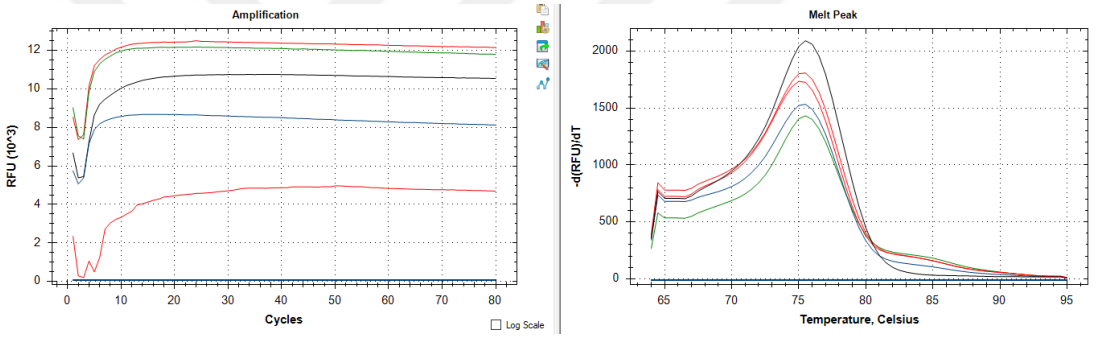

Figure 16 The result of trying 68,8 °C in temperature optimization. The amplification plot at 68,8 °C is shown as a line graph of relative fluorescence units (RFU) values versus cycles (left). The melting curve peak points at 68,8 °C are shown as a line graph of the time-dependent derivative of relative fluorescence units (-d(RFU)/dT) values versus temperatures (right). The samples represented by red, blue, green and black respectively indicate patients, carriers, healthy and blank solution.

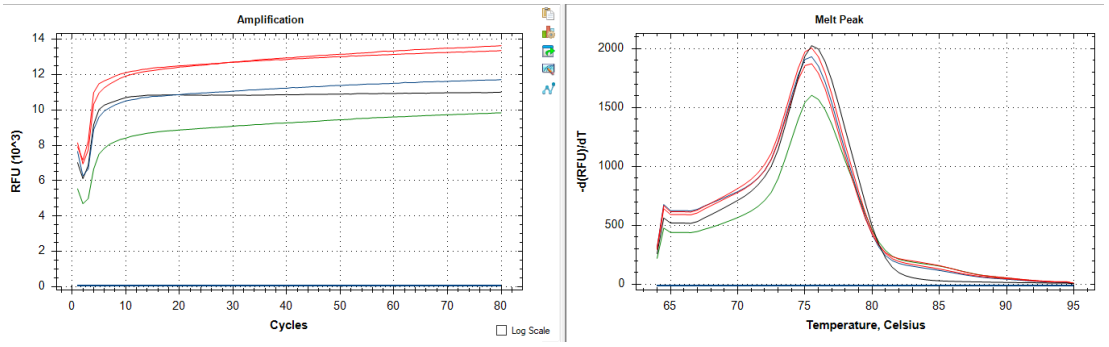

Figure 17 The result of trying 67,4 °C in temperature optimization. The amplification plot at 67,4 °C is shown as a line graph of relative fluorescence units (RFU) values versus cycles (left). The melting curve peak points at 67,4 °C are shown as a line graph of the time-dependent derivative of relative fluorescence units (-d(RFU)/dT) values versus temperatures (right). The samples represented by red, blue, green and black respectively indicate patients, carriers, healthy and blank solution.

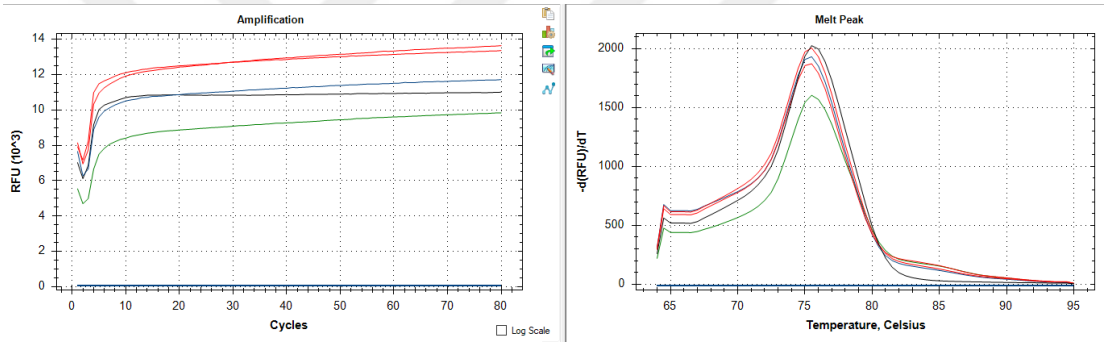

Figure 18 The result of trying 65,7 °C in temperature optimization. The amplification plot at 65,7 °C is shown as a line graph of relative fluorescence units (RFU) values versus cycles (left). The melting curve peak points at 65,7 °C are shown as a line graph of the time-dependent derivative of relative fluorescence units (-d(RFU)/dT) values versus temperatures (right). The samples represented by red, blue, green and black respectively indicate patients, carriers, healthy and blank solution.

When the results of LAMP reactions performed at temperatures of 64,4 °C, 62 °C, 60 °C, 58 °C were examined, it was seen that the melt peak graphs were very close to each other. Melt peak graphs showed increases between 80 °C and 85 °C, distinguishing between patient and healthy samples. As expected, samples from healthy individuals have the highest curve, while samples from patients individuals have lower curves (Figure 19 – Figure 22). Amplification curves were examined to decide which of these temperatures was most appropriate. As a result, 64,4 °C, which

is the temperature at which amplification was highest in the positive control, was chosen as the optimum temperature (Figure 19). This temperature was used for the reactions in the subsequent optimization stages.

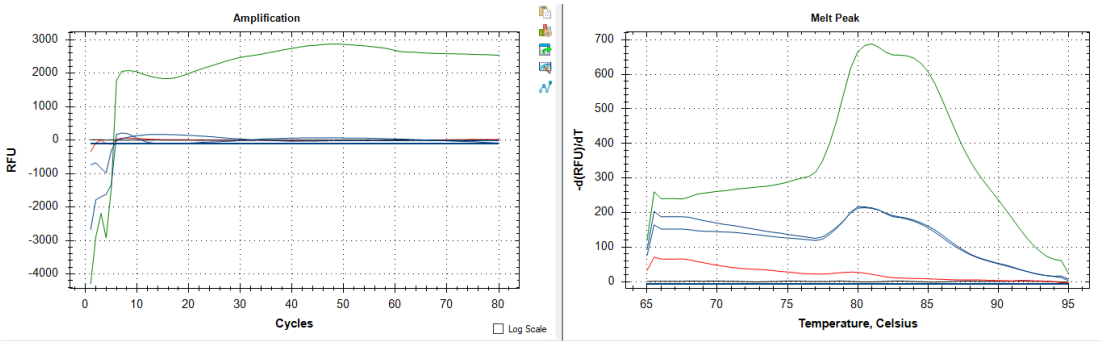

Figure 19 The result of trying 64,4 °C in temperature optimization. The amplification plot at 64,4 °C is shown as a line graph of relative fluorescence units (RFU) values versus cycles (left). The melting curve peak points at 64,4 °C are shown as a line graph of the time-dependent derivative of relative fluorescence units (-d(RFU)/dT) values versus temperatures (right). The samples represented by red, blue, green and black respectively indicate patients, carriers, healthy and blank solution.

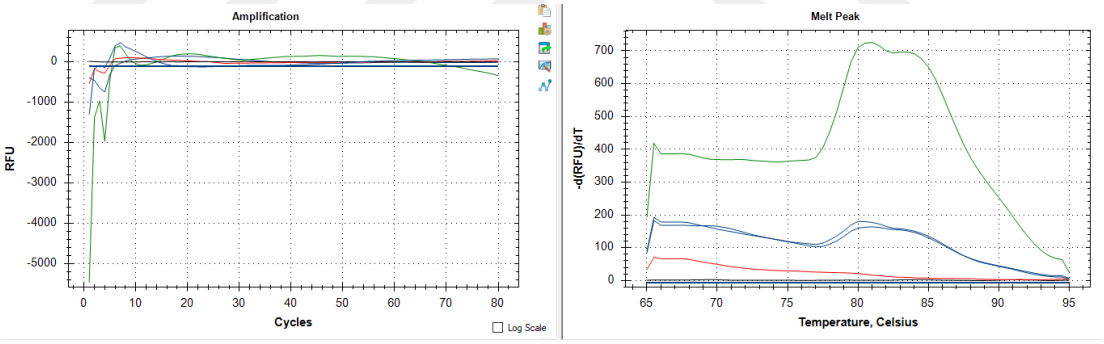

Figure 20 The result of trying 62 °C in temperature optimization. The amplification plot at 62 °C is shown as a line graph of relative fluorescence units (RFU) values versus cycles (left). The melting curve peak points at 62 °C are shown as a line graph of the time-dependent derivative of relative fluorescence units (-d(RFU)/dT) values versus temperatures (right). The samples represented by red, blue, green and black respectively indicate patients, carriers, healthy and blank solution.

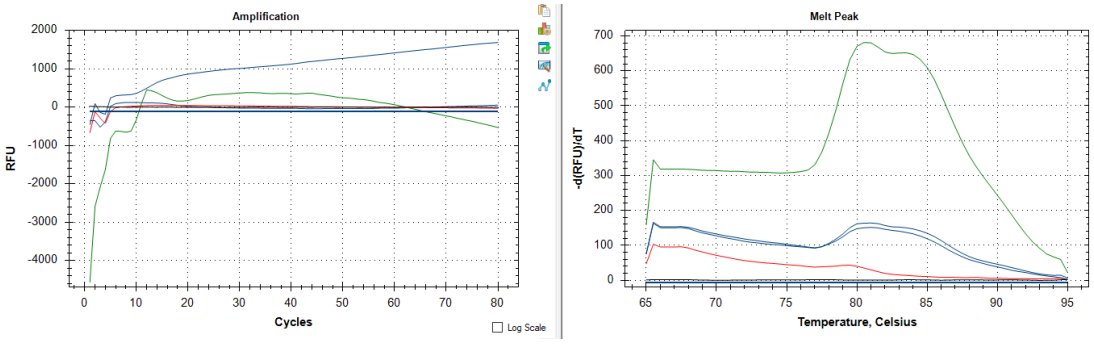

Figure 21 The result of trying 60 °C in temperature optimization. The amplification plot at 60 °C is shown as a line graph of relative fluorescence units (RFU) values versus cycles (left). The melting curve peak points at 60 °C are shown as a line graph of the time-dependent derivative of relative fluorescence units (-d(RFU)/dT) values versus temperatures (right). The samples represented by red, blue, green and black respectively indicate patients, carriers, healthy and blank solution.

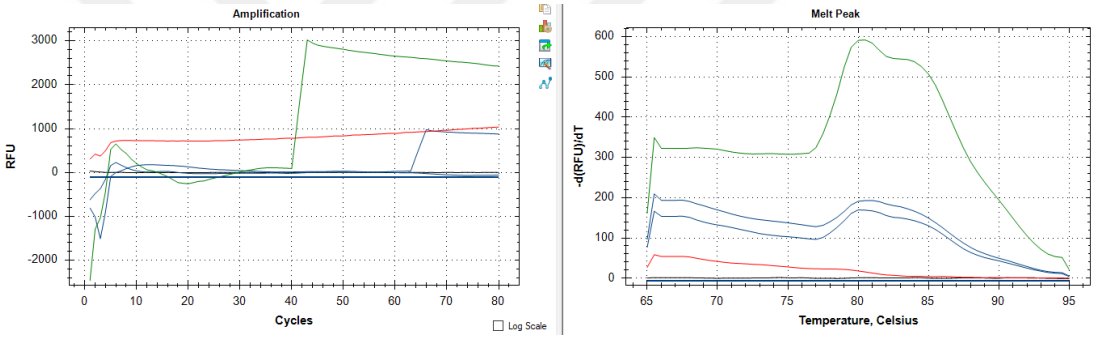

Figure 22 The result of trying 58 °C in temperature optimization. The amplification plot at 58 °C is shown as a line graph of relative fluorescence units (RFU) values versus cycles (left). The melting curve peak points at 58 °C are shown as a line graph of the time-dependent derivative of relative fluorescence units (-d(RFU)/dT) values versus temperatures (right). The samples represented by red, blue, green and black respectively indicate patients, carriers, healthy and blank solution.

Contrary to expectations, there was amplification in patient samples at temperatures of 55,9 °C and 54 °C, but no amplification was observed in healthy individuals (Figure 23, Figure 24).

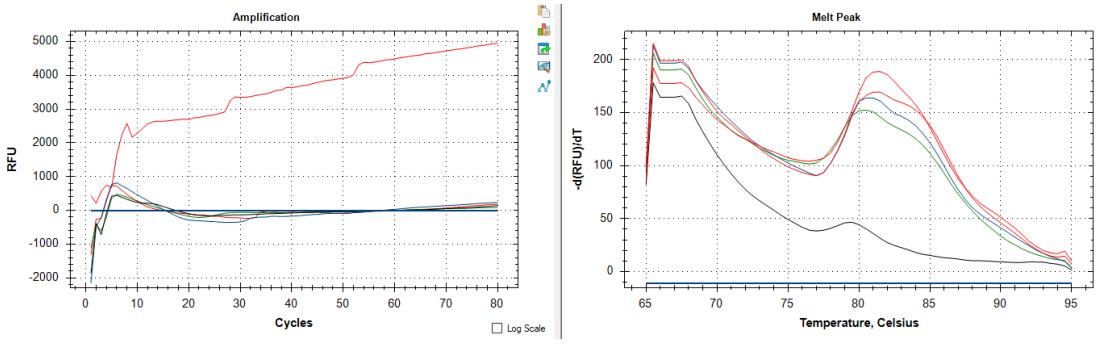

Figure 23 The result of trying 55,9 °C in temperature optimization. The amplification plot at 55,9 °C is shown as a line graph of relative fluorescence units (RFU) values versus cycles (left). The melting curve peak points at 55,9 °C are shown as a line graph of the time-dependent derivative of relative fluorescence units (-d(RFU)/dT) values versus temperatures (right). The samples represented by red, blue, green and black respectively indicate patients, carriers, healthy and blank solution.

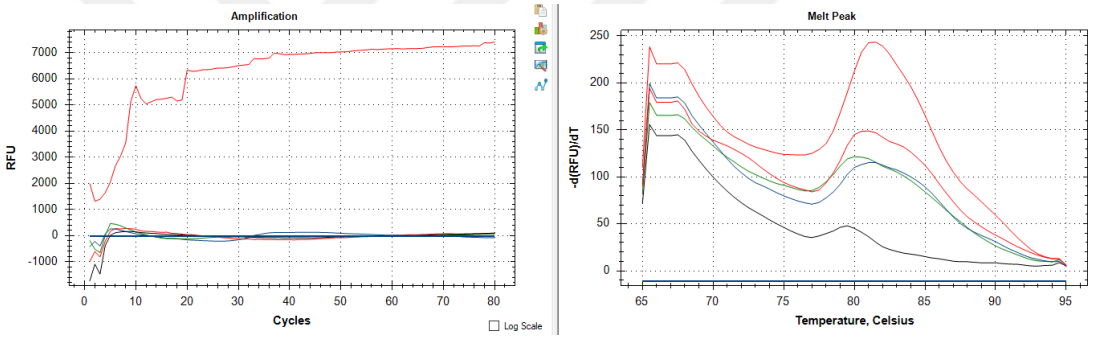

Figure 24 The result of trying 54 °C in temperature optimization. The amplification plot at 54 °C is shown as a line graph of relative fluorescence units (RFU) values versus cycles (left). The melting curve peak points at 54 °C are shown as a line graph of the time-dependent derivative of relative fluorescence units (-d(RFU)/dT) values versus temperatures (right). The samples represented by red, blue, green and black respectively indicate patients, carriers, healthy and blank solution.

At 52 °C, the amplification curves are highest in samples from healthy individuals, followed by carriers, as expected, and there is no amplification in samples from patients. However, when the increases in the melt peak graph are examined, it is not possible to distinguish between patient, healthy and carrier samples (Figure 25).

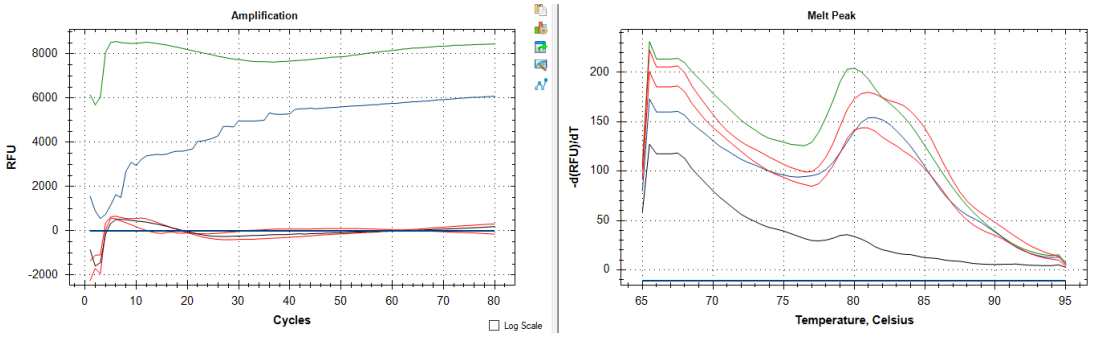

Figure 25 The result of trying 52 °C in temperature optimization. The amplification plot at 52 °C is shown as a line graph of relative fluorescence units (RFU) values versus cycles (left). The melting curve peak points at 52 °C are shown as a line graph of the time-dependent derivative of relative fluorescence units (-d(RFU)/dT) values versus temperatures (right). The samples represented by red, blue, green and black respectively indicate patients, carriers, healthy and blank solution.

Looking at the RT-LAMP result graphs at 50 °C, which is the lowest among the temperatures tested, there was no increase in the amplification graph in the samples of healthy individuals. In addition, in the melt peak graph, the elevations of the samples of patients, carriers and healthy individuals could not be distinguished from each other between 80 °C and 85 °C (Figure 26). It was decided that this temperature value was not suitable for the LAMP system.

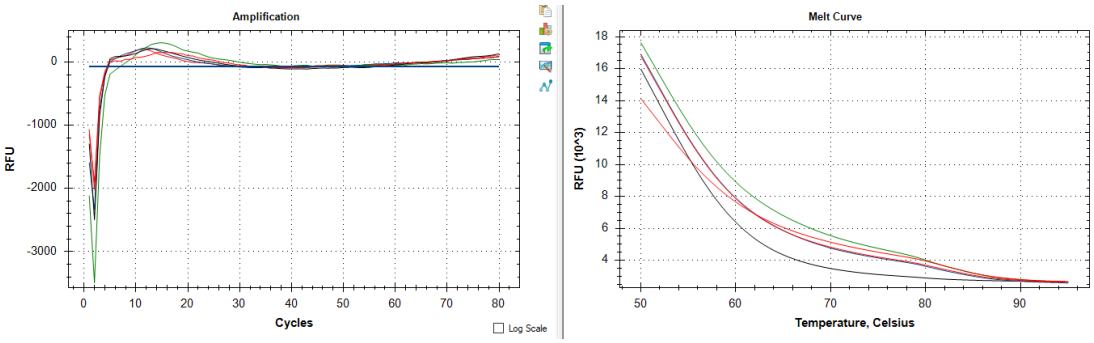

Figure 26 The result of trying 50 °C in temperature optimization. The amplification plot at 50 °C is shown as a line graph of relative fluorescence units (RFU) values versus cycles (left). The melting curve peak points at 50 °C are shown as a line graph of the time-dependent derivative of relative fluorescence units (-d(RFU)/dT) values versus temperatures (right). The samples represented by red, blue, green and black respectively indicate patients, carriers, healthy and blank solution.

4.5.2. $MgSO_4$ Concentration Optimization

In the LAMP reaction using *Bst* enzyme, the amount of $MgSO_4$ normally used was reduced by 30% and the results were examined. When the RT LAMP result graphs were examined, contrary to expectations, there were high amplification curves in patients and carriers, while no amplification was observed in the samples of healthy individuals. In the melt peak graph, the derivation of the samples of healthy individuals between 80 °C and 85 °C was higher than the other samples, as expected, but the derivation curves of the carrier and patient samples could not be distinguished from each other (Figure 27). As a result, changing the $MgSO_4$ concentration reduces the amplification of the positive control. It also brings the curve peaks of the patient and carriers closer to each other between 80 °C and 85 °C.

In the LAMP reaction using *Bst* enzyme, the amount of $MgSO_4$ normally used was increased by 30%. In the melt peak graph, the derivation of the samples of healthy individuals between 80 °C and 85 °C was not higher than the other samples, as expected and the derivation curves of the carrier and patient samples could not be distinguished from each other (Figure 28). As a result, changing the $MgSO_4$ concentration reduces the amplification of the positive control. It also brings the curve peaks of the healthy, patient and carriers closer to each other between 80 °C and 85 °C. Therefore, it does not distinguish between patient, carrier and healthy samples. In subsequent reactions, LAMP reactions were carried out with the previously used $MgSO_4$ concentration.

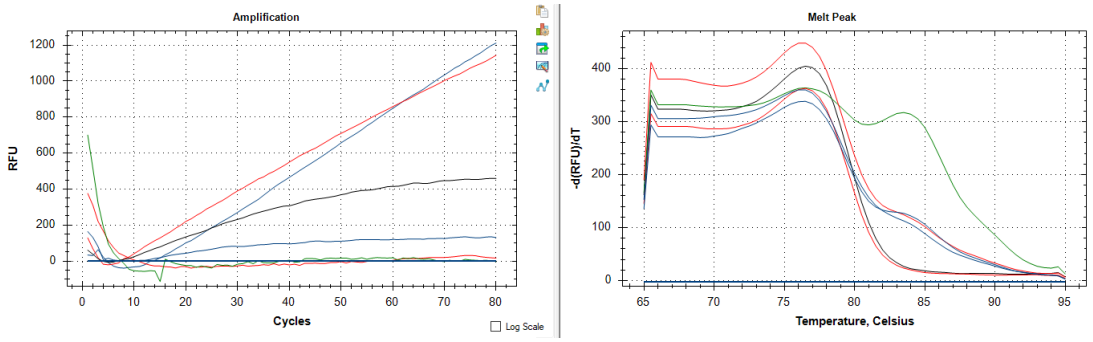

Figure 27 Result of $MgSO_4$ concentration optimization**.** The amplification plot of the diluted $MgSO_4$ reaction mixture is shown as a line graph of relative fluorescence units (RFU) values versus cycles (left). The melting curve peak points of the diluted $MgSO_4$ reaction mixture are shown as a line graph of the time-dependent derivative of relative fluorescence units (-d(RFU)/dT) values versus temperatures (right). The samples represented by red, blue, green and black respectively indicate patients, carriers, healthy and blank solution.

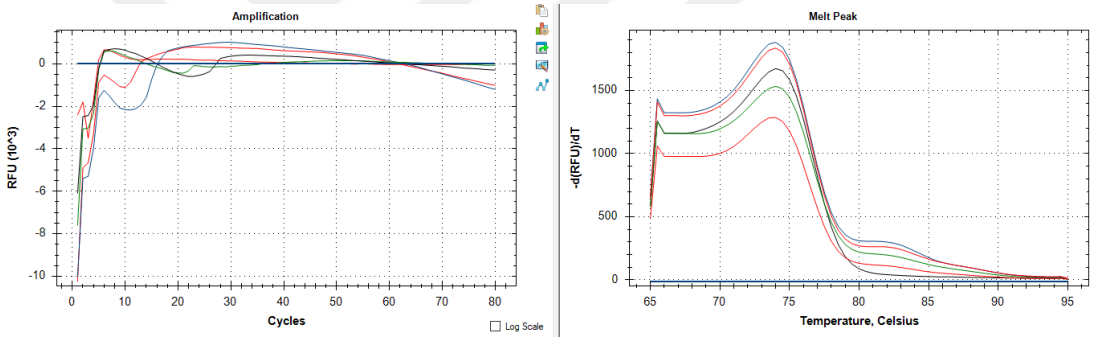

Figure 28 Result of $MgSO_4$ concentration optimization**.** The amplification plot of the diluted $MgSO_4$ reaction mixture is shown as a line graph of relative fluorescence units (RFU) values versus cycles (left). The melting curve peak points of the diluted $MgSO_4$ reaction mixture are shown as a line graph of the time-dependent derivative of relative fluorescence units (-d(RFU)/dT) values versus temperatures (right). The samples represented by red, blue, green and black respectively indicate patients, carriers, healthy and blank solution.

4.6. Validation of the Selected Primer Set

Validation of Primer Pairs via RT-PCR Amplification

In the validation of the primers as a pair set, it was shown that all primers amplified the DNA of the samples (Figure 29 – Figure 32). Since the targeted mutation was not

found in the F3 and B3 primers, as expected, very similar amplification curves were obtained in the samples of patient and healthy individuals in the PCR performed with the F3 - B3 primer set (Figure 29).

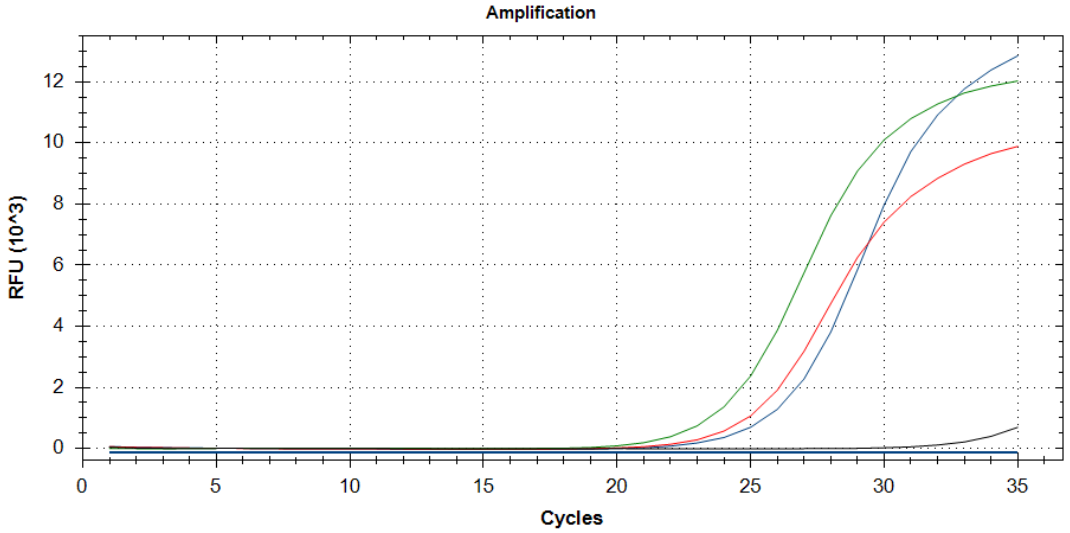

Figure 29 The amplification plot of the F3 – B3 primer pair is shown as a line graph of relative fluorescence units (RFU) values versus cycles. The samples represented by red, blue, green and black respectively indicate patients, carriers, healthy and blank solution.

Since the targeted mutation was not found in the FIP and BIP primers, as expected, very similar amplification curves were obtained in the samples of patient and healthy individuals in the PCR performed with the FIP - BIP primer set (Figure 30).

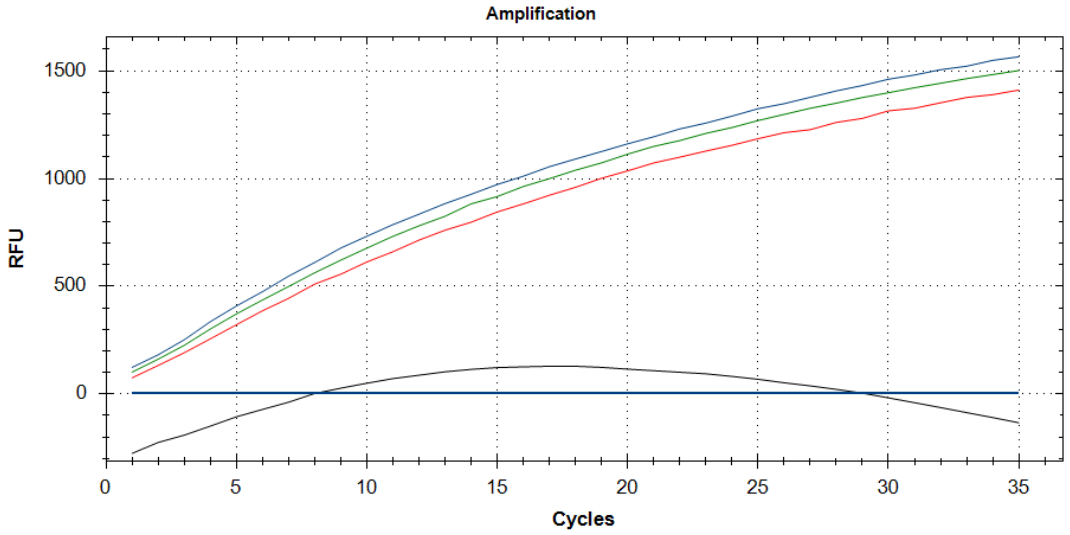

Figure 30 The amplification plot of the FIB – BIP primer pair is shown as a line graph of relative fluorescence units (RFU) values versus cycles. The samples represented by red, blue, green and black respectively indicate patients, carriers, healthy and blank solution.

Although the targeted mutation is not in the F3 primer, it is present in the LoopF primer, so as expected, different amplification curves were obtained in the samples of patient and healthy individuals in the PCR performed with the F3 - LoopF primer set. The healthy individual sample has a higher amplification curve (Figure 31).

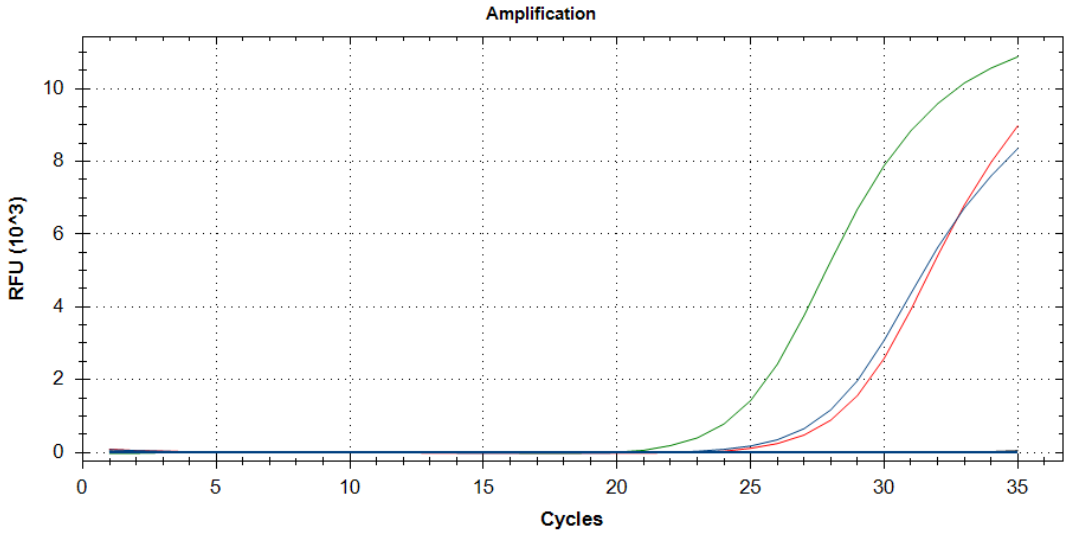

Figure 31 The amplification plot of the F3 - LoopF primer pair is shown as a line graph of relative fluorescence units (RFU) values versus cycles. The samples represented by red, blue, green and black respectively indicate patients, carriers, healthy and blank solution.

Since the targeted mutation was not found in the B3 and LoopB primers, as expected, very similar amplification curves were obtained in the samples of patient and healthy individuals in the PCR performed with the B3 - LoopB primer set (Figure 32).

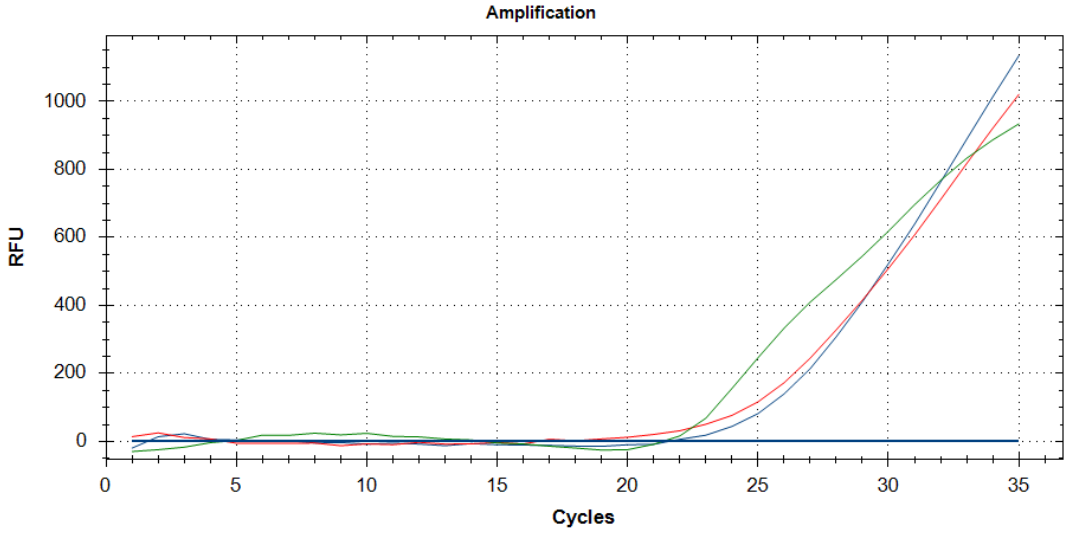

Figure 32 The amplification plot of the B3 - LoopB primer pair is shown as a line graph of relative fluorescence units (RFU) values versus cycles. The samples represented by red, blue, green and black respectively indicate patients, carriers, healthy and blank solution.

4.7. Testing and Comparing DNA Samples Obtained from Blood and Saliva

In the trials conducted with samples of 4 carriers, 5 patients, and 3 patient individuals, the use of DNA obtained from saliva and blood samples in the SMA screening kit was tested and evaluated. Figure 33 shows the separate results of saliva and blood samples of carrier individuals. Figure 34 shows the separate results of saliva and blood samples of patient individuals. Figure 35 shows the separate results of saliva and blood samples of healthy individuals. When the results were examined, it was determined that the tests performed with DNA obtained from blood and saliva samples gave either the same or very similar results.

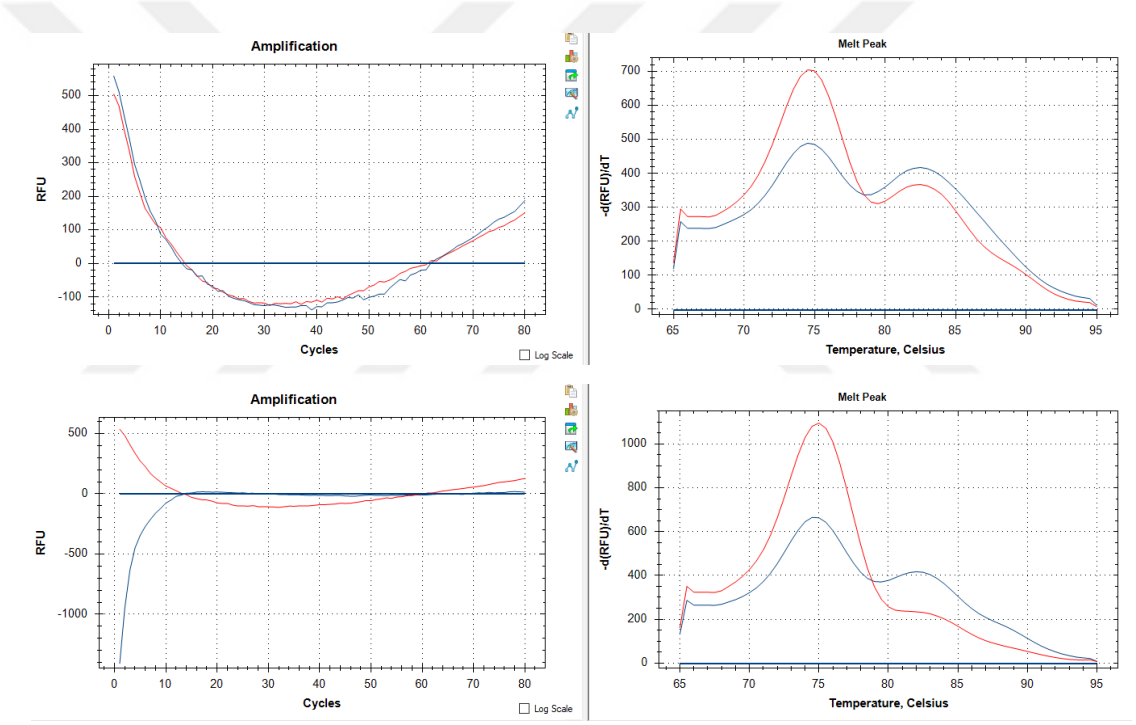

Figure 33 Results of testing and comparing DNA samples obtained from blood and saliva samples with *Bst* enzyme and second primer sets. The amplification plot with all samples is shown as a line graph of relative fluorescence units (RFU) values versus cycles (left). The melting curve peak points with all samples are shown as a line graph of the time-dependent derivative of relative fluorescence units (-d(RFU)/dT) values versus temperatures (right). The samples represented by red and blue respectively indicate DNA samples obtained from the blood samples of the carrier individuals and DNA samples obtained from the saliva samples of the carrier individuals.

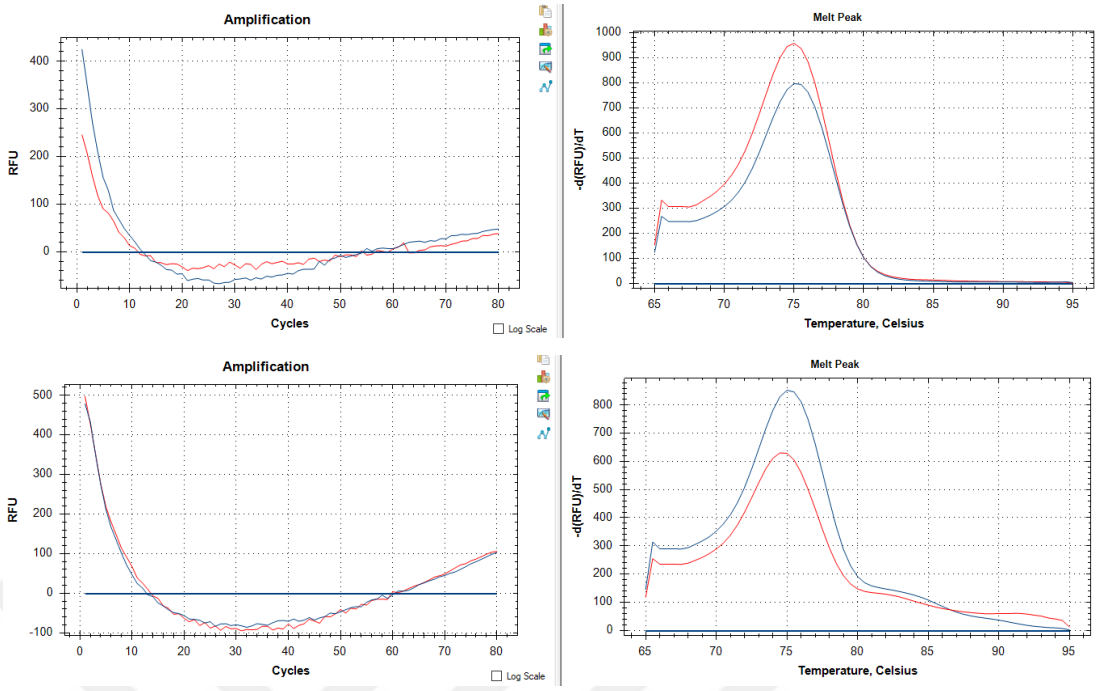

Figure 34 Results of testing and comparing DNA samples obtained from blood and saliva samples with *Bst* enzyme and second primer sets. The amplification plot with all samples is shown as a line graph of relative fluorescence units (RFU) values versus cycles (left). The melting curve peak points with all samples are shown as a line graph of the time-dependent derivative of relative fluorescence units (-d(RFU)/dT) values versus temperatures (right). The samples represented by red and blue respectively indicate DNA samples obtained from the blood samples of the patient individuals and DNA samples obtained from the saliva samples of the patient individuals.

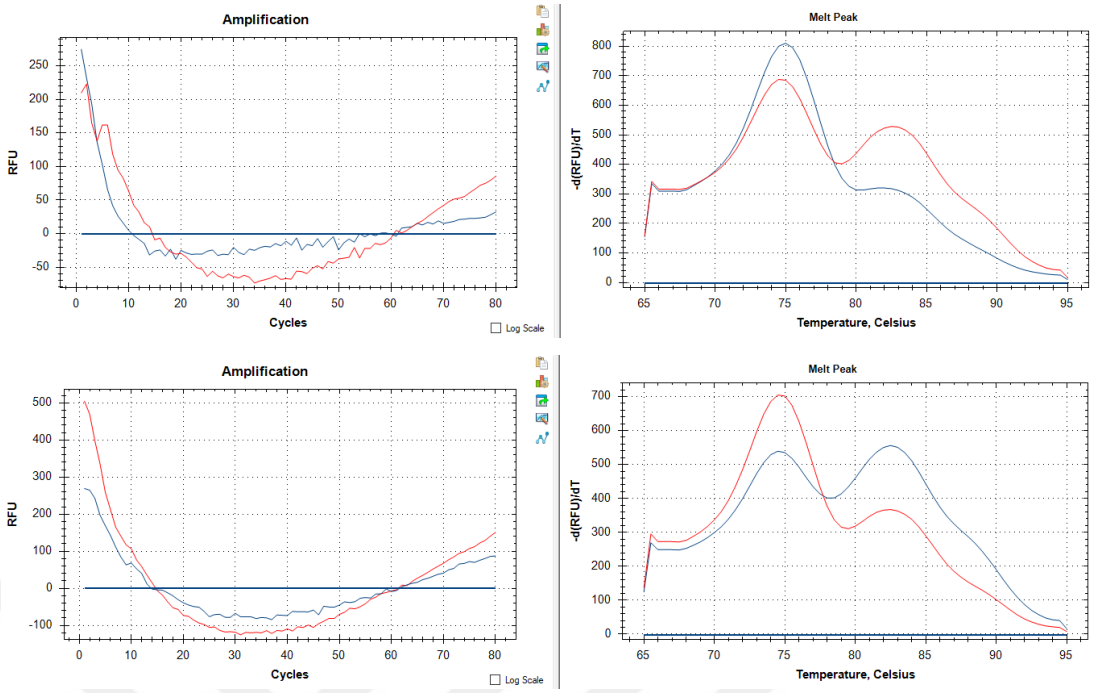

Figure 35 Results of testing and comparing DNA samples obtained from blood and saliva samples with *Bst* enzyme and second primer sets. The amplification plot with all samples is shown as a line graph of relative fluorescence units (RFU) values versus cycles (left). The melting curve peak points with all samples are shown as a line graph of the time-dependent derivative of relative fluorescence units (-d(RFU)/dT) values versus temperatures (right). The samples represented by red and blue respectively indicate DNA samples obtained from the blood samples of the healthy individuals and DNA samples obtained from the saliva samples of the healthy individuals.

4.8. The RT LAMP Results with Patient, Carrier, and Positive Controls

All samples included 18 patients, 16 carriers, and 18 healthy individual. With the developed screening kit, samples of patients with exon 7 deletion or patients with SMN1:c.840C>T rs1164325688 genotype (14 people), carriers (14 people) and healthy individuals (15 people) could be detected completely accurately by looking at the curves between 80 °C and 85 °C in the melt peak graph (Figure 36).

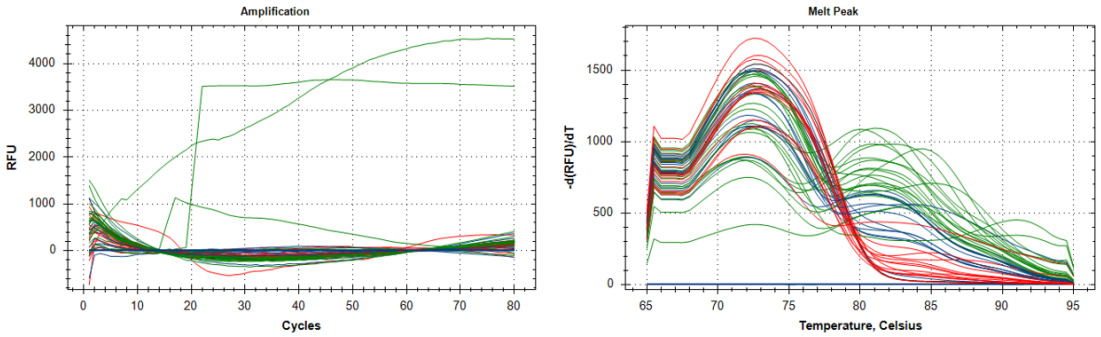

Figure 36 Results of testing samples collectively with *Bst* enzyme and second primer sets. The amplification plot with all samples is shown as a line graph of relative fluorescence units (RFU) values versus cycles (left). The melting curve peak points with all samples are shown as a line graph of the time-dependent derivative of relative fluorescence units (-d(RFU)/dT) values versus temperatures (right). The samples represented by red, blue, green and black respectively indicate patients, carriers, healthy and blank solution.

4.9. Statistical Analysis

Statistical analysis was performed with the total results obtained from the experiments. Sensitivity was found to be 82,35%, specificity was 83,33%, disease prevalence was 65,38%, positive predictive value was 90,32%, negative predictive value was 71,43%, and accuracy was 82,69% The values found were evaluated according to the confidence interval (Table 10).

Table 10 Statistical Calculation Results and Confidence Interval Values

Statistic	**Value**	**95% Confidence Interval**
Sensitivity	82,35%	65,47% to 93,24%
Specificity	83,33%	58,58% to 96,42%
Disease prevalence	65,38%	50,91% to 78,03%
Positive Predictive Value	90,32%	76,65% to 96,37%
Negative Predictive Value	71,43%	54,02% to 84,17%
Accuracy	82,69%	69,67% to 91,77%

Statistical analysis was performed with the total results obtained from the experiments. Patients and carriers were considered a single positive group, and healthy ones were considered negative. As a result of this, true positive rate was found to be 53,85%, false positive rate was 5,77%, false negative rate was 11,54%, true negative rate was 28,85% (Figure 37).

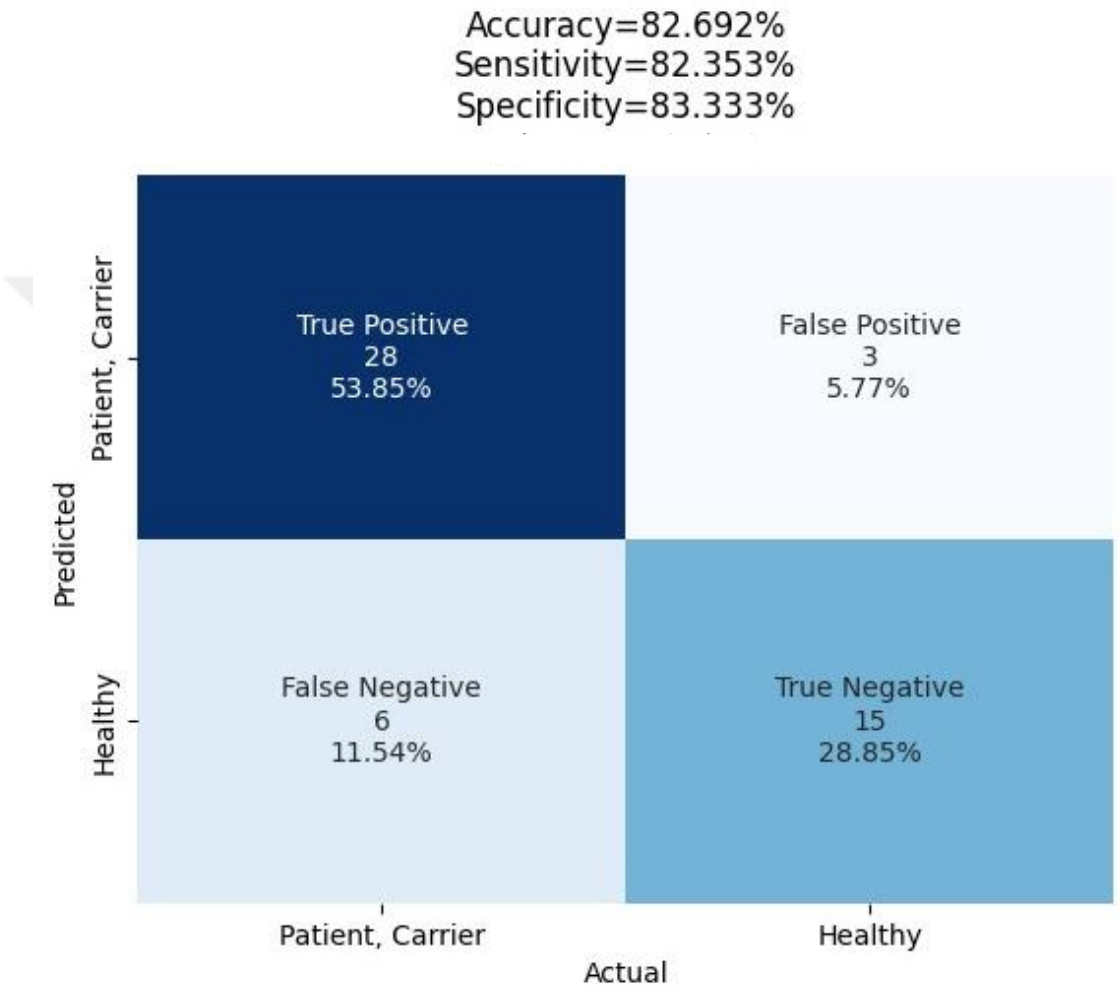

Figure 37 Confusion matrix of the cohort

Of the group of 34 samples which were carriers and patients, 28 samples were found to be correctly positive. 6 of these 34 samples were found to be negative in test results. 15 out of 18 healthy samples were detected as negative in the test results, and 3 samples were detected as positive (Figure 38).

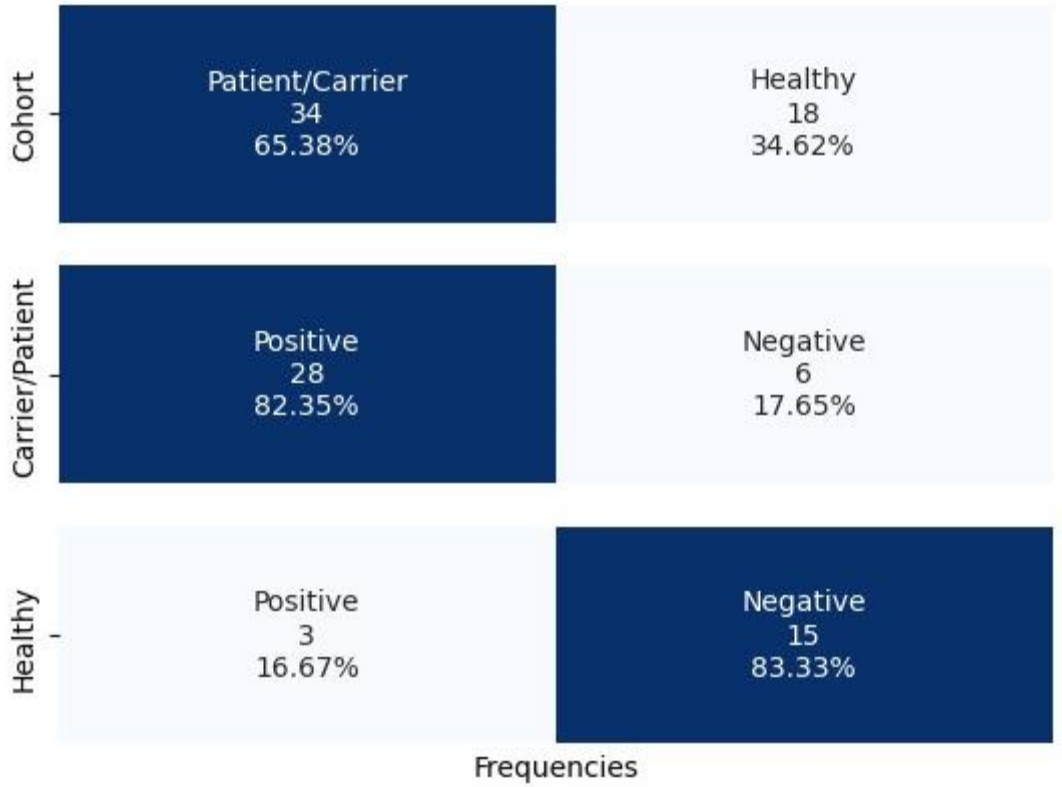

Figure 38 Sums of the confusion matrix

5. DISCUSSION

Muscle atrophy and weakness are common in SMA disease. This can cause the veins to become thinner and deeper, making them harder to find (139). SMA is usually diagnosed in infants and young children. It is generally more difficult to find a vein in these age groups because the veins are smaller and children may move around more due to their fear of needles (140). When the results of the experiments in which DNA samples obtained from blood and saliva samples taken from patient, carriers and healthy individuals were comparatively tested, it was found appropriate to use saliva samples instead of blood samples. Considering these, the results obtained from the study will provide great convenience in taking samples from individuals with SMA.

Another relevant research paper explores RT LAMP for SARS CoV 2 detection without requiring saliva extraction (141). This research stresses the importance of straightforward and cost effective tests during pandemics. While the RT qPCR method is used as a gold standard for diagnosing SARS CoV 2 infection it is time intensive emphasizing the necessity for methods such as LAMP for rapid disease identification. Collectively these studies underscore the potential and efficiency of using LAMP based approaches, in disease detection.

The cost-effectiveness of the LAMP method is another critical advantage. LAMP tests for SMA cost approximately $20 to $50, significantly lower than MLPA ($400 to $800) and PCR ($100 to $300) (142-145). By reducing the need for expensive reagents and equipment, this approach makes SMA screening accessible to a broader population, which is crucial for public health initiatives focusing on widespread carrier screening and early diagnosis.

The application of LAMP based techniques, in disease detection on obtainable samples like saliva shows promise for advancing early disease diagnosis and monitoring. Recent advancements in this field have proven the efficacy of LAMP based tests in identifying diseases, viral infections such as SARS CoV 2. For example the Rapid COVID 19 LAMP assay employs a metallochromic detection system utilizing zinc ions and a zinc sensor to address the limitations of LAMP approaches (146). This presents a sensitive test with four layers showcasing how adaptable and sensitive LAMP based methods are in detecting pathogens. This highlights the application of LAMP based techniques in identifying mutations linked to conditions like SMA.

During the project 3 different primer sets needed for LAMP reactions were developed which were fine tuned to amplify the target mutation in the SMN1 gene. The stability of the designed primers, such as the intrinsic capability of forming dimers, were thoroughly investigated to optimize reaction conditions.

Since the optimum temperature range required for the LAMP reaction to occur is between 60 °C and 65 °C, care was taken to ensure that the melting temperatures of the designed primers were within this range (147). As a result of the experiments performed with the first, second and third primer sets, it was decided that the second primer set could best detect the targeted mutation and exon deletion with the LAMP system.

In the literature, it is emphasized that the Tm values of LAMP primers are generally in the range of 60 - 65°C (147). In the second primer set, melting temperature (Tm) values are between 50,3 ºC and 63 ºC. These temperatures enabled the primers

to bind tightly to the target DNA sequence and increase the efficiency of the reaction.

Hairpin Tm generally refers to the self-folding temperature of the primer and should ideally be lower than Tm (147). Accordingly, in the second primer set, Hairpin Tm values were lower than Tm values. Hairpin Tm value was taken into account to prevent hairpin formation among the primers or on the target DNA sequence.

It is emphasized in the literature that LAMP primers are generally 18 - 25 nucleotides in length (147). In the second primer set, primers F1, F2, F3, B1, B2, B3 are approximately the recommended length of 18-25 nucleotides. This length enabled the primers to bind specifically and effectively to the target DNA sequence.

The ideal GC content should generally be between 40 % and 60 % (148), while in the second primer set it is between 22,2 % and 33,3 %. It was taken into account that the GC content may vary depending on the characteristics of the target DNA sequence and the primer design, and it is more important to ensure that the primers target the target DNA specifically and efficiently. Therefore, the GC content was taken into account during the design, but since the GC content was not in the ideal range, the locations of the primers were not changed by moving them outside the targeted gene regions.

The second primer set met the necessary criteria for this: melting temperature, hairpin Tm, and length of the primers. The fact that the targeted mutation in the second primer set was in the LoopF primer provided an advantage in terms of making the

primer specific.

Furthermore tasks like selecting enzymes optimizing temperatures, for LAMP reactions and adjusting MgSO4 concentration were carried out. *Bst* DNA polymerase stands out as an used enzyme, in the LAMP system due to its attributes. Known for its tolerance this enzyme enables LAMP reactions to take place under conditions. It functions effectively across a temperature range of 55 °C – 65 °C and a pH range of 6 - 9. An intriguing feature of *Bst* DNA polymerase is its " activity " allowing synthesis and removal of DNA segments facilitating self propagation in LAMP reactions. Compared to DNA polymerases *Bst* DNA polymerase is notably swift expediting LAMP reactions. These qualities led to the inclusion of *Bst* DNA polymerase, in the optimization phase (149-151). Using the *Bst* enzyme helped distinguish between patient and carrier samples accurately. Primer pairs validation was done through binary RT-PCR amplification. Among the designed primer sets, the second primer set gave the best results in LAMP reactions with *Bst* enzyme, as expected. It was determined that the second primer set worked best at 64,4 °C, which is the appropriate temperature range for the LAMP system, in LAMP reactions carried out with the *Bst* enzyme.

It is known that when RT-LAMP is performed on samples obtained from patients, carriers and healthy individuals in the LAMP system, it is recommended to reduce the amount of $MgSO_4$ in some studies (152) in order to better distinguish the samples from each other in the melt peak graph and to obtain clear results. Contrary to previous studies, reducing the $MgSO_4$ ratio in this study did not yield a better result.

This study effectively demonstrated that the second primer set could distinguish individuals with the SMN1;c.840C>T rs1164325688 variation among patients.

Utilizing this primer set, diagnosed several patients and achieved significant results. In this project, tested a total of 16 samples from carrier individuals, 18 samples from SMA-diagnosed patients, and 18 samples from healthy individuals. The kit successfully identified 14 out of 18 patients and 14 out of 16 carriers, while accurately identifying 15 out of 18 healthy individuals. This translated to a sensitivity of 82,35%, a specificity of 83,3%, PPV of 90,32%, NPV of 71,43% and accuracy of 82,69%. Sensitivity, specificity, and accuracy are calculated as percentages. Confidence intervals for sensitivity, specificity, and accuracy are computed using the "exact" Clopper-Pearson method (153-155). This method provides more accurate confidence intervals, especially for smaller sample sizes. Confidence intervals for the positive and negative predictive values are derived using standard logit confidence intervals (156). In cases where the predictive value is either 0% or 100%, a Clopper-Pearson confidence interval is reported. This approach ensures robustness in the estimation of predictive values under extreme conditions (157-159). By utilizing these statistical methods, the study ensures the reliability and accuracy of the reported diagnostic performance metrics. These calculations provide a comprehensive understanding of the screening test's efficacy in identifying healthy, carrier, and patient groups.

The high specificity underscores the kit's reliability in ruling out non-SMA individuals, while the moderate sensitivity indicates room for improvement in detecting all affected patients and carriers. Notably, 87,5% of known carriers were correctly identified, highlighting the methodology's effectiveness in carrier screening. These promising results, achieved using only the second primer set, suggest that this set has high potential for SMA diagnosis and carrier screening.

Despite the successful identification of many carriers and patients, the kit did not work for individuals with mutations outside the targeted region. Future research aims to design primers covering all variants, enabling comprehensive screening for all SMA

patients and carriers using multiple primer sets.

The challenge in reaching more SMA samples was due to the severe medical conditions of Type 1 patients. Once the sample size increases under appropriate conditions, the validation of the screening kit will be completed, enhancing the test kit's accuracy.

Plans are underway to publish these findings in a scientific journal and secure a patent for commercializing the kit. One of the main advantages of the LAMP-based kit is its simplicity and rapid turnaround time. Unlike traditional methods, the LAMP reaction completes within 30 to 40 minutes and does not require advanced equipment. This makes it highly suitable for various environments, including resource-limited settings. The use of saliva samples further enhances the kit's accessibility, eliminating the need for invasive sample collection methods.

Given the success of this kit in detecting SMA, there is potential for its application in screening for other genetic disorders. The adaptability of the LAMP technology, combined with its efficiency and cost-effectiveness, makes it a promising tool for various genetic screening programs.

6. CONCLUSION

In conclusion, development of a LAMP-based screening kit for Spinal Muscular Atrophy represents a significant breakthrough in genetic diagnostics. By leveraging saliva samples, this innovative kit addresses the key limitations of traditional methods like MLPA and PCR, which are often costly, time-consuming, and require specialized equipment and expertise. Our results demonstrate that the newly developed kit is both efficient and accurate in detecting SMA patients and carriers, specifically targeting the SMN1 gene mutation c.840C>T. This non-invasive, rapid, and cost-effective tool has shown high specificity and overall efficiency, making it a valuable asset in early SMA diagnosis and carrier screening. While the current sensitivity could be enhanced, the promising outcomes of this study highlight the kit's potential to revolutionize SMA detection. In this study, fluorometric assay was optimized in the LAMP system. It is aimed to carry out optimization studies for LAMP fluorometric assay directly from saliva samples without DNA isolation and sample preparation. For the future studies, it will be aimed to optimize the colorimetric assay in the LAMP system by using thermal cyclers. Future research will focus on optimizing its sensitivity and exploring its applicability to other genetic disorders, ultimately contributing to improved public health outcomes and enhanced patient care.

7. REFERENCES

1. Mercuri, E., Sumner, C. J., Muntoni, F., Darras, B. T., & Finkel, R. S. (2022). Spinal muscular atrophy. Nature Reviews Disease Primers, 8(1), 52.

2. Zhang, Y., Odiwuor, N., Xiong, J., Sun, L., Nyaruaba, R. O., Wei, H., & Tanner, N. A. (2020). Rapid molecular detection of SARS-CoV-2 (COVID-19) virus RNA using colorimetric LAMP. MedRxiv, 2020-02.
3. Talbot, K., & Tizzano, E. F. (2017). The clinical landscape of spinal muscular atrophy: Where do we stand and where are we going? Annual Review of Neuroscience.
4. Mercuri, E., Sumner, C.J., Muntoni, F. et al. Spinal muscular atrophy. Nat Rev Dis Primers 8, 52 (2022). https://doi.org/10.1038/s41572-022-00380-8
5. Little, D., et al. (2010). Frequency and distribution of SMA types in a large North American population. Neuromuscular Disorders.
6. Mendonca, R. H., et al. (2019). Spinal muscular atrophy type 0: A case report and review of the literature. Pediatric Neurology
7. Mercuri, E., Sumner, C.J., Muntoni, F. et al. Spinal muscular atrophy. Nat Rev Dis Primers 8, 52 (2022). https://doi.org/10.1038/s41572-022-00380-8
8. Ogino, S., Leonard, D. G., Rennert, H., Ewens, W. J. & Wilson, R. B. Genetic risk assessment in carrier testing for spinal muscular atrophy. Am. J. Med. Genet. 110, 301–307 (2002).
9. Pearn, J. Incidence, prevalence, and gene frequency studies of chronic childhood spinal muscular atrophy. J. Med. Genet. 15, 409–413 (1978).
10. Sugarman, E. A. et al. Pan-ethnic carrier screening and prenatal diagnosis for spinal muscular atrophy: clinical laboratory analysis of >72,400 specimens. Eur. J. Hum. Genet. 20, 27–32 (2012).
11. Mailman, M. D. et al. Molecular analysis of spinal muscular atrophy and modification of the phenotype by SMN2. Genet. Med. 4, 20–26 (2002).
12. M L Mostacciuolo 1, G A Danieli, C Trevisan, E Müller, C Angelini. Epidemiology of spinal muscular atrophies in a sample of the Italian population. Neuroepidemiology 1992;11(1):34-8.
13. A Thieme 1, B Mitulla, F Schulze, A W Spiegler. Epidemiological data on Werdnig-Hoffmann disease in Germany (West-Thüringen) Hum Genet 1993;91(3):295-7.
14. Darras BT. Spinal muscular atrophies. Pediatr Clin North Am. 2015;62(3):743-66.
15. Ministry of Health of the Republic of Turkey. (2019). Spinal muscular atrofi (SMA) kılavuzu [Spinal Muscular Atrophy (SMA) Guideline]. Retrieved from https://shgmargestddb.saglik.gov.tr/Eklenti/43881/0/smakp190822pdf.pdf
16. Lefebvre, S. et al. Identification and characterization of a spinal muscular atrophy-determining gene. Cell 80, 155–165 (1995).
17. Lefebvre, S. et al. Correlation between severity and SMN protein level in spinal muscular

atrophy. Nat. Genet. 16, 265–269 (1997).

18. Lorson, C. L. & Androphy, E. J. An exonic enhancer is required for inclusion of an essential exon in the SMA-determining gene SMN. Hum. Mol. Genet. 9, 259–265 (2000).
19. Lorson, C. L., Hahnen, E., Androphy, E. J. & Wirth, B. A single nucleotide in the SMN gene regulates splicing and is responsible for spinal muscular atrophy. Proc. Natl Acad. Sci. USA 96, 6307–6311 (1999).
20. Monani, U. R. et al. A single nucleotide difference that alters splicing patterns distinguishes the SMA gene SMN1 from the copy gene SMN2. Hum. Mol. Genet. 8, 1177–1183 (1999).
21. Wirth, B. Spinal muscular atrophy: in the challenge lies a solution. Trends Neurosci. 44, 306–322 (2021). This comprehensive review discusses the evolution over the past 25 years in the understanding of the pathobiology of SMA, genotype–phenotype relationships and treatment strategies.
22. van der Steege, G. et al. Apparent gene conversions involving the SMN gene in the region of the spinal muscular atrophy locus on chromosome 5. Am. J. Hum. Genet. 59, 834–838 (1996).
23. Echaniz-Laguna, A., Miniou, P., Bartholdi, D. & Melki, J. The promoters of the survival motor neuron gene (SMN) and its copy (SMNc) share common regulatory elements. Am. J. Hum. Genet. 64, 1365–1370 (1999).
24. Jodelka, F. M., Ebert, A. D., Duelli, D. M. & Hastings, M. L. A feedback loop regulates splicing of the spinal muscular atrophy-modifying gene, SMN2. Hum. Mol. Genet. 19, 4906–4917 (2010).
25. Monani, U. R., McPherson, J. D. & Burghes, A. H. Promoter analysis of the human centromeric and telomeric survival motor neuron genes (SMNC and SMNT). Biochim. Biophys. Acta 1445, 330–336 (1999).
26. Kernochan, L. E. et al. The role of histone acetylation in SMN gene expression. Hum. Mol. Genet. 14, 1171–1182 (2005).
27. Farooq, F. et al. Prolactin increases SMN expression and survival in a mouse model of severe spinal muscular atrophy via the STAT5 pathway. J. Clin. Invest. 121, 3042–3050 (2011).
28. McCormack, N. M. et al. A high-throughput genome-wide RNAi screen identifies modifiers of survival motor neuron protein. Cell Rep. 35, 109125 (2021).
29. Marasco, L. E. et al. Counteracting chromatin effects of a splicing-correcting antisense oligonucleotide improves its therapeutic efficacy in spinal muscular atrophy. Cell 185, 2057–2070.e15 (2022).
30. Woo, C. J. et al. Gene activation of SMN by selective disruption of lncRNA-mediated recruitment of PRC2 for the treatment of spinal muscular atrophy. Proc. Natl Acad. Sci. USA 114, E1509–E1518 (2017).
31. d'Ydewalle, C. et al. The antisense transcript SMN-AS1 regulates SMN expression and is a novel therapeutic target for spinal muscular atrophy. Neuron 93, 66–79 (2017).

32. Ottesen, E. W., Seo, J., Singh, N. N. & Singh, R. N. A multilayered control of the human survival motor neuron gene expression by Alu elements. Front. Microbiol. 8, 2252 (2017).
33. Avila, A. M. et al. Trichostatin A increases SMN expression and survival in a mouse model of spinal muscular atrophy. J. Clin. Invest. 117, 659–671 (2007).
34. Lorson, C. L., Hahnen, E., Androphy, E. J. & Wirth, B. A single nucleotide in the SMN gene regulates splicing and is responsible for spinal muscular atrophy. Proc. Natl Acad. Sci. USA 96, 6307–6311 (1999).
35. Monani, U. R. et al. A single nucleotide difference that alters splicing patterns distinguishes the SMA gene SMN1 from the copy gene SMN2. Hum. Mol. Genet. 8, 1177–1183 (1999).
36. Cartegni, L. & Krainer, A. R. Disruption of an SF2/ASF-dependent exonic splicing enhancer in SMN2 causes spinal muscular atrophy in the absence of SMN1. Nat. Genet. 30, 377–384 (2002).
37. Kashima, T. & Manley, J. L. A negative element in SMN2 exon 7 inhibits splicing in spinal muscular atrophy. Nat. Genet. 34, 460–463 (2003).
38. Singh, R. N. & Singh, N. N. Mechanism of splicing regulation of spinal muscular atrophy genes. Adv. Neurobiol. 20, 31–61 (2018).
39. Prior, T. W. et al. A positive modifier of spinal muscular atrophy in the SMN2 gene. Am. J. Hum. Genet. 85, 408–413 (2009).
40. Wu, X. et al. A-44G transition in SMN2 intron 6 protects patients with spinal muscular atrophy. Hum. Mol. Genet. 26, 2768–2780 (2017).
41. Auslander, N. et al. The GENDULF algorithm: mining transcriptomics to uncover modifier genes for monogenic diseases. Mol. Syst. Biol. 16, e9701 (2020).
42. Ruggiu, M. et al. A role for SMN exon 7 splicing in the selective vulnerability of motor neurons in spinal muscular atrophy. Mol. Cell Biol. 32, 126–138 (2012).
43. Prior, T. W. et al. Newborn and carrier screening for spinal muscular atrophy. Am. J. Med. Genet. A 152A, 1608–1616 (2010).
44. Feldkotter, M., Schwarzer, V., Wirth, R., Wienker, T. F. & Wirth, B. Quantitative analyses of SMN1 and SMN2 based on real-time lightCycler PCR: fast and highly reliable carrier testing and prediction of severity of spinal muscular atrophy. Am. J. Hum. Genet. 70, 358–368 (2002).
45. Calucho, M. et al. Correlation between SMA type and SMN2 copy number revisited: an analysis of 625 unrelated Spanish patients and a compilation of 2834 reported cases. Neuromuscul. Disord. 28, 208–215 (2018). A detailed genotpe–phenotype analysis of the Spanish SMA population is presented, melded with a comprehensive literature review.
46. Arkblad, E., Tulinius, M., Kroksmark, A. K., Henricsson, M. & Darin, N. A population-based study of genotypic and phenotypic variability in children with spinal muscular atrophy. Acta Paediatr. 98, 865–872 (2009).
47. Prior, T. W., Swoboda, K. J., Scott, H. D. & Hejmanowski, A. Q. Homozygous SMN1 deletions in unaffected family members and modification of the phenotype by SMN2. Am.

J. Med. Genet. A 130A, 307–310 (2004).

48. Oprea, G. E. et al. Plastin 3 is a protective modifier of autosomal recessive spinal muscular atrophy. Science 320, 524–527 (2008).
49. Riessland, M. et al. Neurocalcin delta suppression protects against spinal muscular atrophy in humans and across species by restoring impaired endocytosis. Am. J. Hum. Genet. 100, 297–315 (2017).
50. Kaifer, K. A. et al. Plastin-3 extends survival and reduces severity in mouse models of spinal muscular atrophy. JCI Insight 2, e89970 (2017).
51. Mailman, M. D. et al. Molecular analysis of spinal muscular atrophy and modification of the phenotype by SMN2. Genet. Med. 4, 20–26 (2002).
52. Prior, T. W. et al. A positive modifier of spinal muscular atrophy in the SMN2 gene. Am. J. Hum. Genet. 85, 408–413 (2009).
53. Singh, R. N., Howell, M. D., Ottesen, E. W. & Singh, N. N. Diverse role of survival motor neuron protein. Biochim. Biophys. Acta Gene Regul. Mech. 1860, 299–315 (2017). This comprehensive review discusses the many roles of SMN protein in RNA metabolism.
54. Le, T. T. et al. SMNΔ7, the major product of the centromeric survival motor neuron (SMN2) gene, extends survival in mice with spinal muscular atrophy and associates with full-length SMN. Hum. Mol. Genet. 14, 845–857 (2005).
55. Burnett, B. G. et al. Regulation of SMN protein stability. Mol. Cell Biol. 29, 1107–1115 (2009).
56. Cho, S. & Dreyfuss, G. A degron created by SMN2 exon 7 skipping is a principal contributor to spinal muscular atrophy severity. Genes Dev. 24, 438–442 (2010).
57. Kwon, D. Y. et al. The E3 ubiquitin ligase mind bomb 1 ubiquitinates and promotes the degradation of survival of motor neuron protein. Mol. Biol. Cell 24, 1863–1871 (2013).
58. Powis, R. A. et al. Systemic restoration of UBA1 ameliorates disease in spinal muscular atrophy. JCI Insight 1, e87908 (2016).
59. Riboldi, G. M. et al. Sumoylation regulates the assembly and activity of the SMN complex. Nat. Commun. 12, 5040 (2021).
60. Renvoise, B., Querol, G., Verrier, E. R., Burlet, P. & Lefebvre, S. A role for protein phosphatase PP1γ in SMN complex formation and subnuclear localization to Cajal bodies. J. Cell Sci. 125, 2862–2874 (2012).
61. Han, K. J. et al. Monoubiquitination of survival motor neuron regulates its cellular localization and Cajal body integrity. Hum. Mol. Genet. 25, 1392–1405 (2016).
62. Grimmler, M. et al. Phosphorylation regulates the activity of the SMN complex during assembly of spliceosomal U snRNPs. EMBO Rep. 6, 70–76 (2005).
63. Petri, S., Grimmler, M., Over, S., Fischer, U. & Gruss, O. J. Dephosphorylation of survival motor neurons (SMN) by PPM1G/PP2Cγ governs Cajal body localization and stability of the SMN complex. J. Cell Biol. 179, 451–465 (2007).
64. Coovert, D. D. et al. The survival motor neuron protein in spinal muscular atrophy. Hum.

Mol. Genet. 6, 1205–1214 (1997).

65. Zhang, H. et al. Multiprotein complexes of the survival of motor neuron protein SMN with Gemins traffic to neuronal processes and growth cones of motor neurons. J. Neurosci. 26, 8622–8632 (2006).
66. Donlin-Asp, P. G. et al. The survival of motor neuron protein acts as a molecular chaperone for mRNP assembly. Cell Rep. 18, 1660–1673 (2017).
67. Pellizzoni, L., Yong, J. & Dreyfuss, G. Essential role for the SMN complex in the specificity of snRNP assembly. Science 298, 1775–1779 (2002).
68. Tisdale, S. et al. SMN is essential for the biogenesis of U7 small nuclear ribonucleoprotein and 3'-end formation of histone mRNAs. Cell Rep. 5, 1187–1195 (2013).
69. Winkler, C. et al. Reduced U snRNP assembly causes motor axon degeneration in an animal model for spinal muscular atrophy. Genes Dev. 19, 2320–2330 (2005).
70. Zhang, Z. et al. SMN deficiency causes tissue-specific perturbations in the repertoire of snRNAs and widespread defects in splicing. Cell 133, 585–600 (2008).
71. Fallini, C., Donlin-Asp, P. G., Rouanet, J. P., Bassell, G. J. & Rossoll, W. Deficiency of the survival of motor neuron protein impairs mRNA localization and local translation in the growth cone of motor neurons. J. Neurosci. 36, 3811–3820 (2016).
72. Rossoll, W. et al. Smn, the spinal muscular atrophy-determining gene product, modulates axon growth and localization of β-actin mRNA in growth cones of motoneurons. J. Cell Biol. 163, 801–812 (2003).
73. Donlin-Asp, P. G., Bassell, G. J. & Rossoll, W. A role for the survival of motor neuron protein in mRNP assembly and transport. Curr. Opin. Neurobiol. 39, 53–61 (2016).
74. Hao le, T. et al. HuD and the survival motor neuron protein interact in motoneurons and are essential for motoneuron development, function, and mRNA regulation. J. Neurosci. 37, 11559–11571 (2017).
75. Akten, B. et al. Interaction of survival of motor neuron (SMN) and HuD proteins with mRNA cpg15 rescues motor neuron axonal deficits. Proc. Natl Acad. Sci. USA 108, 10337–10342 (2011).
76. Strasswimmer, J. et al. Identification of survival motor neuron as a transcriptional activator-binding protein. Hum. Mol. Genet. 8, 1219–1226 (1999).
77. Lauria, F. et al. SMN-primed ribosomes modulate the translation of transcripts related to spinal muscular atrophy. Nat. Cell Biol. 22, 1239–1251 (2020).
78. Oprea, G. E. et al. Plastin 3 is a protective modifier of autosomal recessive spinal muscular atrophy. Science 320, 524–527 (2008).
79. Riessland, M. et al. Neurocalcin delta suppression protects against spinal muscular atrophy in humans and across species by restoring impaired endocytosis. Am. J. Hum. Genet. 100, 297–315 (2017).
80. Kaifer, K. A. et al. Plastin-3 extends survival and reduces severity in mouse models of spinal muscular atrophy. JCI Insight 2, e89970 (2017).

81. Torres-Benito, L. et al. NCALD antisense oligonucleotide therapy in addition to nusinersen further ameliorates spinal muscular atrophy in mice. Am. J. Hum. Genet. 105, 221–230 (2019).
82. Upadhyay, A. et al. Neurocalcin delta knockout impairs adult neurogenesis whereas half reduction is not pathological. Front. Mol. Neurosci. 12, 19 (2019).
83. Wolff, L. et al. Plastin 3 in health and disease: a matter of balance. Cell Mol. Life Sci. 78, 5275–5301 (2021).
84. Miller, N., Shi, H., Zelikovich, A. S. & Ma, Y. C. Motor neuron mitochondrial dysfunction in spinal muscular atrophy. Hum. Mol. Genet. 25, 3395–3406 (2016).
85. Boyd, P. J. et al. Bioenergetic status modulates motor neuron vulnerability and pathogenesis in a zebrafish model of spinal muscular atrophy. PLoS Genet. 13, e1006744 (2017).
86. Thelen, M. P., Wirth, B. & Kye, M. J. Mitochondrial defects in the respiratory complex I contribute to impaired translational initiation via ROS and energy homeostasis in SMA motor neurons. Acta Neuropathol. Commun. 8, 223 (2020).
87. Ripolone, M. et al. Impaired muscle mitochondrial biogenesis and myogenesis in spinal muscular atrophy. JAMA Neurol. 72, 666–675 (2015).
88. Habets, L. E. et al. Magnetic resonance reveals mitochondrial dysfunction and muscle remodelling in spinal muscular atrophy. Brain https://doi.org/10.1093/brain/awab411 (2021).
89. Wadman, R. I. et al. A comparative study of SMN protein and mRNA in blood and fibroblasts in patients with spinal muscular atrophy and healthy controls. PLoS ONE 11, e0167087 (2016).
90. Poirier, A. et al. Risdiplam distributes and increases SMN protein in both the central nervous system and peripheral organs. Pharmacol. Res. Perspect. 6, e00447 (2018).
91. Burlet, P. et al. The distribution of SMN protein complex in human fetal tissues and its alteration in spinal muscular atrophy. Hum. Mol. Genet. 7, 1927–1933 (1998).
92. Ramos, D. M. et al. Age-dependent SMN expression in disease-relevant tissue and implications for SMA treatment. J. Clin. Invest. 129, 4817–4831 (2019). Human fetal and infant autopsy samples from both unaffected individuals and those with SMA were analysed for SMN protein and transcript levels. SMN protein expression is highest in late fetal and early postnatal development.
93. Gabanella, F., Carissimi, C., Usiello, A. & Pellizzoni, L. The activity of the spinal muscular atrophy protein is regulated during development and cellular differentiation. Hum. Mol. Genet. 14, 3629–3642 (2005).
94. Ji, C. et al. Interaction of 7SK with the Smn complex modulates snRNP production. Nat. Commun. 12, 1278 (2021).
95. Gavrilina, T. O. et al. Neuronal SMN expression corrects spinal muscular atrophy in severe SMA mice while muscle-specific SMN expression has no phenotypic effect. Hum. Mol. Genet. 17, 1063–1075 (2008).

96. Van Alstyne, M. et al. Gain of toxic function by long-term AAV9-mediated SMN overexpression in the sensorimotor circuit. Nat. Neurosci. 24, 930–940 (2021). This study examined overexpression of SMN in a mouse model of SMA via AAV9–SMN gene transduction and identified chronic development of sensory and motor impairment.
97. Thomsen, G. et al. Biodistribution of onasemnogene abeparvovec DNA, mRNA and SMN protein in human tissue. Nat. Med. 27, 1701–1711 (2021).
98. Ling, K. K., Lin, M. Y., Zingg, B., Feng, Z. & Ko, C. P. Synaptic defects in the spinal and neuromuscular circuitry in a mouse model of spinal muscular atrophy. PLoS ONE 5, e15457 (2010).
99. Mentis, G. Z. et al. Early functional impairment of sensory-motor connectivity in a mouse model of spinal muscular atrophy. Neuron 69, 453–467 (2011). Experiments in a mouse model for SMA support the authors' proposal that SMA is a poly-neuronal network disorder, not purely a disease of motor neurons.
100. Fletcher, E. V. et al. Reduced sensory synaptic excitation impairs motor neuron function via Kv2.1 in spinal muscular atrophy. Nat. Neurosci. 20, 905–916 (2017).
101. Kong, L. et al. Impaired prenatal motor axon development necessitates early therapeutic intervention in severe SMA. Sci. Transl. Med. https://doi.org/10.1126/scitranslmed.abb6871 (2021). Human autopsy samples from infants with SMA type 1 were studied for axonal development and demonstrated features of developmental arrest, followed by neurodegeneration, suggesting that there is a narrow therapeutic window to rescue the motor neurons after birth.
102. Kariya, S. et al. Reduced SMN protein impairs maturation of the neuromuscular junctions in mouse models of spinal muscular atrophy. Hum. Mol. Genet. 17, 2552–2569 (2008). Studies on the neuromuscular junction in a mouse model of severe SMA demonstrated early presynaptic morphological changes and functional impairment.
103. Murray, L. M. et al. Selective vulnerability of motor neurons and dissociation of pre- and post-synaptic pathology at the neuromuscular junction in mouse models of spinal muscular atrophy. Hum. Mol. Genet. 17, 949–962 (2008).
104. Kong, L. et al. Impaired synaptic vesicle release and immaturity of neuromuscular junctions in spinal muscular atrophy mice. J. Neurosci. 29, 842–851 (2009).
105. Lee, Y. I., Mikesh, M., Smith, I., Rimer, M. & Thompson, W. Muscles in a mouse model of spinal muscular atrophy show profound defects in neuromuscular development even in the absence of failure in neuromuscular transmission or loss of motor neurons. Dev. Biol. 356, 432–444 (2011).
106. Kizina, K. et al. Cognitive impairment in adult patients with 5q-associated spinal muscular atrophy. Brain Sci. https://doi.org/10.3390/brainsci11091184 (2021).
107. Masson, R., Brusa, C., Scoto, M. & Baranello, G. Brain, cognition, and language development in spinal muscular atrophy type 1: a scoping review. Dev. Med. Child Neurol. 63, 527–536 (2021).

108. Schorling, D. C., Pechmann, A. & Kirschner, J. Advances in treatment of spinal muscular atrophy – new phenotypes, new challenges, new implications for care. J. Neuromuscul. Dis. 7, 1–13 (2020).
109. Montes, J. et al. Nusinersen improves walking distance and reduces fatigue in later-onset spinal muscular atrophy. Muscle Nerve 60, 409–414 (2019).
110. De Vivo, D. C. et al. Nusinersen initiated in infants during the presymptomatic stage of spinal muscular atrophy: interim efficacy and safety results from the phase 2 NURTURE study. Neuromuscul. Disord. 29, 842–856 (2019). Nusinersen is the first of the three SMN-enhancing drugs to demonstrate a marked improvement in survival and function when treatment is started shortly after birth, in the presymptomatic or early symptomatic state of SMA.
111. Schorling, D. C. et al. Discrepancy in redetermination of SMN2 copy numbers in children with SMA. Neurology 93, 267–269 (2019).
112. Boemer, F. et al. Newborn screening for SMA in Southern Belgium. Neuromuscul. Disord. 29, 343–349 (2019).
113. Zhao, S. et al. Next generation sequencing is a highly reliable method to analyze exon 7 deletion of survival motor neuron 1 (SMN1) gene. Sci. Rep. 12, 223 (2022).
114. Darras, B. T. et al. Neurofilament as a potential biomarker for spinal muscular atrophy. Ann. Clin. Transl. Neurol. 6, 932–944 (2019). This study identified elevated plasma phosphorylated neurofilament heavy chain levels in children with SMA compared with typically developing children, which declined under treatment with nusinersen, suggesting that this could serve as an informative prognostic and predictive biomarker.
115. Sugarman, E. A. et al. Pan-ethnic carrier screening and prenatal diagnosis for spinal muscular atrophy: clinical laboratory analysis of >72,400 specimens. Eur. J. Hum. Genet. 20, 27–32 (2012).
116. Gregg, A. R. et al. Screening for autosomal recessive and X-linked conditions during pregnancy and preconception: a practice resource of the American College of Medical Genetics and Genomics (ACMG). Genet. Med. 23, 1793–1806 (2021).
117. Aharoni, S. et al. Impact of a national population-based carrier-screening program on spinal muscular atrophy births. Neuromuscul. Disord. 30, 970–974 (2020).
118. Sun, Y., Kong, X., Zhao, Z. & Zhao, X. Mutation analysis of 419 family and prenatal diagnosis of 339 cases of spinal muscular atrophy in China. BMC Med. Genet. 21, 133 (2020).
119. Almeida-Porada, G. et al. In utero gene therapy consensus statement from the IFeTIS. Mol. Ther. 27, 705–707 (2019).
120. US National Library of Medicine. ClinicalTrials.gov https://clinicaltrials.gov/ct2/show/NCT03761849 (2022).
121. De Vivo, D. C. et al. Nusinersen initiated in infants during the presymptomatic stage of spinal muscular atrophy: interim efficacy and safety results from the phase 2 NURTURE

study. Neuromuscul. Disord. 29, 842–856 (2019). Nusinersen is the first of the three SMN-enhancing drugs to demonstrate a marked improvement in survival and function when treatment is started shortly after birth, in the presymptomatic or early symptomatic state of SMA.

122. Strauss, K. A. et al. Onasemnogene abeparvovec for presymptomatic infants with two copies of SMN2 at risk for spinal muscular atrophy type 1: the phase III SPR1NT trial. Nat. Med. https://doi.org/10.1038/s41591-022-01866-4 (2022).
123. Strauss, K. A. et al. Onasemnogene abeparvovec for presymptomatic infants with three copies of SMN2 at risk for spinal muscular atrophy: the phase III SPR1NT trial. Nat. Med. https://doi.org/10.1038/s41591-022-01867-3 (2022).
124. Wang, C. H. et al. Consensus statement for standard of care in spinal muscular atrophy. J. Child Neurol. 22, 1027–1049 (2007).
125. Finkel, R. S. et al. Diagnosis and management of spinal muscular atrophy: part 2: pulmonary and acute care; medications, supplements and immunizations; other organ systems; and ethics. Neuromuscul. Disord. 28, 197–207 (2018). This revision of the standard-of-care guidelines for SMA provides a template for the comprehensive management of patients with SMA.
126. Mercuri, E. et al. Diagnosis and management of spinal muscular atrophy: part 1: recommendations for diagnosis, rehabilitation, orthopedic and nutritional care. Neuromuscul. Disord. 28, 103–115 (2018). This revision of the standard-of-care guidelines for SMA provides a template for the comprehensive management of patients with SMA.
127. Notomi, T., Mori, Y., Tomita, N., & Kanda, H. (2015). Loop-mediated isothermal amplification (LAMP): principle, features, and future prospects. Journal of microbiology, 53(1), 1-5.
128. New England Biolabs. (n.d.). Loop-mediated isothermal amplification (LAMP). Retrieved from https://www.neb.com/en/applications/dna-amplification-pcr-and-qpcr/isothermal-amplification/loop-mediated-isothermal-amplification-lamp
129. Notomi, T., Okayama, H., Masubuchi, H., Yonekawa, T., Watanabe, K., Amino, N., & Hase, T. (2000). Loop-mediated isothermal amplification of DNA. Nucleic acids research, 28(12), e63. DOI: 10.1093/nar/28.12.e63
130. Nagamine, K., Hase, T., & Notomi, T. (2002). Accelerated reaction by loop-mediated isothermal amplification using loop primers. Molecular and cellular probes, 16(3), 223-229. DOI: 10.1006/mcpr.2002.0415
131. Tomita, N., Mori, Y., Kanda, H., & Notomi, T. (2008). Loop-mediated isothermal amplification (LAMP) of gene sequences and simple visual detection of products. Nature protocols, 3(5), 877-882. DOI: 10.1038/nprot.2008.57
132. Mori, Y., Nagamine, K., Tomita, N., & Notomi, T. (2001). Detection of loop-mediated isothermal amplification reaction by turbidity derived from magnesium pyrophosphate formation. Biochemical and biophysical research communications, 289(1), 150-154. DOI:

10.1006/bbrc.2001.5921

133. Goto, M., Honda, E., Ogura, A., & Nomoto, A. (2009). Loop-mediated isothermal amplification (LAMP) method for rapid detection of Mycobacterium tuberculosis. Journal of clinical microbiology, 45(11), 4095-4099. DOI: 10.1128/JCM.01630-07
134. Clopper, C. J., & Pearson, E. S. (1934). The use of confidence or fiducial limits illustrated in the case of the binomial. Biometrika, 26(4), 404-413.
135. Song, F., Glenny, A. M., & Altman, D. G. (2000). Indirect comparison in evaluating relative efficacy illustrated by antimicrobial prophylaxis in colorectal surgery. Controlled clinical trials, 21(5), 488-497.
136. Mercaldo, N. D., Lau, K. F., & Zhou, X. H. (2007). Confidence intervals for predictive values with an emphasis to case–control studies. Statistics in medicine, 26(10), 2170-2183.
137. Novartis. (n.d.). Newborn screening for spinal muscular atrophy (SMA). Retrieved April 28, 2021, from https://www.novartis.com/our-company/novartis-pharmaceuticals/novartis-gene-therapies/newborn-screening-spinal-muscular-atrophy-sma
138. Liu, Z., Zhang, P., He, X., Liu, S., Tang, S., Zhang, R., ... & Zou, L. (2016). New multiplex real-time PCR approach to detect gene mutations for spinal muscular atrophy. BMC neurology, 16(1), 1-12. Talbot, K., & Tizzano, E. F. (2017). The clinical landscape for SMA in a new therapeutic era. Gene therapy, 24(9), 529-533.
139. Lunn, M. R., & Wang, C. H. (2008). Spinal muscular atrophy. The Lancet, 371(9630), 2120-2133.
140. Kolb, S. J., & Kissel, J. T. (2011). Spinal muscular atrophy: a timely review. Archives of neurology, 68(8), 979-984.
141. Yu, L., Wu, S., Hao, X., Dong, X., Mao, L., Pelechano, V., ... & Zhang, S. (2020). Rapid detection of COVID-19 coronavirus using a reverse transcriptional loop-mediated isothermal amplification (RT-LAMP) diagnostic platform. Clinical Chemistry, 66(7), 975-977.
142. Stuppia L, Antonucci I, Palka G and others. ‘Use of the MLPA assay in the Molecular Diagnosis of Gene Copy Number Alterations in Human Genetic Diseases‘. International Journal of Molecular Sciences 2012: volume 13, issue 3, pages 3,245–3,276. DOI: 10.3390/ijms13033245
143. Stuppia, L., Antonucci, I., Palka, G., & Gatta, V. (2012). Use of the MLPA assay in the molecular diagnosis of gene copy number alterations in human genetic diseases. International journal of molecular sciences, 13(3), 3245-3276.
144. Yao, M., Jiang, L., Yu, Y. *et al.* Optimized MLPA workflow for spinal muscular atrophy diagnosis: identification of a novel variant, NC_000005.10:g.(70919941_70927324)del in isolated exon 1 of *SMN1* gene through long-range PCR. *BMC Neurol* **24**, 93 (2024). https://doi.org/10.1186/s12883-024-03592-5
145. GeneDx. (2024). Spinal muscular atrophy (SMN1/SMN2 deletion/duplication) MLPA. Genetics & Genomics Center. https://ggc.org/test-finder-item/spinal-muscular-atrophy-

smn1-smn2-deletion-duplication-mlpa

146. Szobi, A., Buranovská, K., Vojtaššáková, N., Lovíšek, D., Özbaşak, H. Ö., Szeibeczederová, S., ... & Paul, E. D. (2023). Vivid COVID-19 LAMP is an ultrasensitive, quadruplexed test using LNA-modified primers and a zinc ion and 5-Br-PAPS colorimetric detection system. Communications Biology, 6(1), 233.
147. Becherer, L., Borst, N., Bakheit, M., Frischmann, S., Zengerle, R., & von Stetten, F. (2020). Loop-mediated isothermal amplification (LAMP)–review and classification of methods for sequence-specific detection. Analytical Methods, 12(6), 717-746.
148. Park, J. W. (2022). Principles and applications of loop-mediated isothermal amplification to point-of-care tests. Biosensors, 12(10), 857.
149. Notomi, T., Okayama, H., Masubuchi, H., Yonekawa, T., Watanabe, K., Amino, N., & Hase, T. (2000). Loop-mediated isothermal amplification of DNA. Nucleic acids research, 28(12), E63-E63.
150. Mori, Y., Nagamine, K., Tomita, N., & Notomi, T. (2001). Detection of loop-mediated isothermal amplification reaction by turbidity derived from magnesium pyrophosphate formation. Biochemical and biophysical research communications, 289(1), 150-154.
151. Nagamine, K., Hase, T., & Notomi, T. (2002). Accelerated reaction by loop-mediated isothermal amplification using loop primers. Molecular and Cellular Probes, 16(3), 223-229.
152. Park, J. W. (2022). Principles and applications of loop-mediated isothermal amplification to point-of-care tests. Biosensors, 12(10), 857.
153. Gardner IA, Greiner M (2006) Receiver-operating characteristic curves and likelihood ratios: improvements over traditional methods for the evaluation and application of veterinary clinical pathology tests. Veterinary Clinical Pathology 35:8-17.
154. Griner PF, Mayewski RJ, Mushlin AI, Greenland P (1981) Selection and interpretation of diagnostic tests and procedures. Annals of Internal Medicine 94:555-600.
155. Hanley JA, McNeil BJ (1982) The meaning and use of the area under a receiver operating characteristic (ROC) curve. Radiology 143:29-36.
156. Mercaldo ND, Lau KF, Zhou XH (2007) Confidence intervals for predictive values with an emphasis to case-control studies. Statistics in Medicine 26:2170-2183.
157. Metz CE (1978) Basic principles of ROC analysis. Seminars in Nuclear Medicine 8:283-298.
158. Zhou XH, NA Obuchowski, DK McClish (2002) Statistical methods in diagnostic medicine. New York: Wiley.
159. Zweig MH, Campbell G (1993) Receiver-operating characteristic (ROC) plots: a fundamental evaluation tool in clinical medicine. Clinical Chemistry 39:561-577.

8. CURRICULUM VITAE